# 15. Quark Model

Revised August 2025 by C. Amsler (Marietta Blau Inst.), V. Crede (Florida State U.) and T. DeGrand (Colorado U., Boulder).

15.1	Introduction	1
15.2	Quantum numbers of the quarks	2
15.3	Mesons	3
15.4	Exotic mesons	Ć
	15.4.1 Tetraquarks	10
	15.4.2 Glueballs	11
	15.4.3 Hybrids	12
15.5	Baryons: qqq states	13
	15.5.1 Light baryons	13
	15.5.2 Charmed and bottom baryons	19
15.6	Magnetic moments	23
15.7	Dynamics	25
15.8	Lattice Calculations of Hadronic Spectroscopy	27
	15.8.1 Spectroscopy of low-lying states	28
	15.8.2 Excited state spectroscopy	29
	15.8.3 Electromagnetic effects	35

### 15.1 Introduction

Quantum chromodynamics (QCD) is the theory of strong interactions. QCD is a quantum field theory with an  $SU(N_c)$  local "color" gauge symmetry with  $N_c = 3$  colors and a collection of  $N_f$  "flavors" of colored fermions, the quarks. It involves a set of  $N_c^2 - 1 = 8$  non-Abelian gauge fields, the gluons. QCD is believed to confine, that is, its physical states are color singlets with internal quark and gluon degrees of freedom. This review is concerned with the description of the properties (masses and matrix elements for couplings to electromagnetism and the weak intractions) of the low lying bound states of QCD. The shorthand expression for describing this physics is called the "quark model".

The spectrum of strongly interacting particles consists of a tower of many states, which can be either bosons (labelled as "mesons") or fermions (labelled as "baryons"). The spectrum of baryons and mesons exhibits a high degree of regularity. The organizational principle which best categorizes this regularity is encoded in the quark model. All descriptions of strongly interacting states use the language of the quark model. At the same time, the language is not precise. The quark model exists on many levels: at the simplest level, it is an almost dynamics-free picture of strongly interacting particles as bound states of quarks and antiquarks. As one refines the description, the quark model can become a framework with more detailed descriptions of dynamics. At its most fundamental level, it might be a description of QCD. In effective field theories of QCD at low energies the hadron spectrum is not simply given by a series of states but is the manifestation of a complex dynamics involving various types of states [1].

At its heart, the quark model assumes that mesons are bound states of quark - antiquark pairs, and baryons are bound states of three quarks. These are the minimal particle content states which can be color singlets in an SU(3) gauge theory. This approach cannot be justified directly from

QCD; however, there is indirect evidence that this description has some fundamental validity from the version of QCD where the number of colors  $N_c$  is taken to infinity [2–4]. In that limit, mesons are dominantly narrow (width proportional to  $1/N_c$ ) bound states of a quark - antiquark pair, and baryons have a mass which scales as  $N_c$ .

A better justification is that this approach works. Indeed, the quark model is much older than QCD as a theory of the strong interactions (1973-1974, see the article on "50 Years of Quantum Chromodynamics" [5]). In fact, the principal issue (circa 1963-64) in strong interaction physics before QCD was to justify the success of the quark model in systemizing the properties of mesons and baryons in terms of some more fundamental dynamics (QCD).

Today one knows that this is not the whole story. There are experimentally observed states which either cannot be described, or have an uncomfortable description, as minimal quark number states. Some of them have "exotic" (non- $\bar{q}q$  or qqq) quantum numbers. Given the successes of the quark model, these are classified as "tetraquarks" ( $qq\bar{q}\bar{q}$ ), "pentaquarks" ( $qqqq\bar{q}$ ) or "glueballs", bound states of gluons, the gluonic degrees of freedom in QCD. Of course, such labels are imprecise: bound states with the same overall quantum numbers can mix, regardless of their internal degrees of freedom.

This review has several parts. We start by describing the properties of strongly interacting particles in terms of the properties of states made of a minimal number of quark fields which can be coupled into a color singlet – two fields (a quark and an antiquark) for the mesons, and three quarks, for a baryon. Quarks come in six flavors. We describe the properties of mesons as  $\bar{q}q$  systems and baryons as qqq systems. Along the way we discuss hadronic bound states which do not fit into this classification.

Finally, at the end of this review, we present results from lattice simulations of QCD, a direct approach to the solution of QCD from its Lagrangian, without reference to models. Lattice simulations interact with the quark model in (at least) two ways: first, the interpolating fields which are used in lattice simulations are usually directly based on quark model constructions. That is the simplest way to create states with the desired quantum numbers, which can then be processed by the lattice calculation. The second way that lattice calculations interact with the quark model comes when one wishes to put the lattice calculations into some context: without the quark model, there are simply the results from the lattice calculations, and the results from experiment, and no way to understand why they are similar or different. The quark model is the framework which is almost universally used to generate that context. Of course, that statement is equally valid when one tries to systemize actual experimental data: the context is always some variation of a quark model.

### 15.2 Quantum numbers of the quarks

As gluons carry no intrinsic quantum numbers beyond color charge, and because color is believed to be permanently confined, the quantum numbers of strongly interacting particles are given by the quantum numbers of their constituent quarks and antiquarks.

Quarks are strongly interacting fermions with spin 1/2 and, by convention, positive parity. Antiquarks have negative parity. Quarks have the additive baryon number 1/3, antiquarks -1/3. Table 15.1 gives the other additive quantum numbers (flavors) for the three generations of quarks. They are related to the charge Q (in units of the elementary charge e) through the generalized Gell-Mann-Nishijima formula

$$Q = I_z + \frac{B + S + C + B + T}{2}, \qquad (15.1)$$

where  $\mathcal{B}$  is the baryon number. The convention is that the quark flavor ( $I_z$ , S, C, B, or T) has the same sign as its charge Q. Antiquarks have the opposite flavor signs. With this convention,

any flavor carried by a charged meson has the same sign as its charge, e.g., the strangeness of the  $K^+$   $(u\bar{s})$  is +1, the bottomness of the  $B^+$   $(u\bar{b})$  is +1, and the charm and strangeness of the  $D_s^ (s\bar{c})$  are each -1.

	d	u	s	c	b	$\overline{t}$
Q – electric charge	$-\frac{1}{3}$	$+\frac{2}{3}$	$-\frac{1}{3}$	$+\frac{2}{3}$	$-\frac{1}{3}$	$+\frac{2}{3}$
I – isospin	$\frac{1}{2}$	$\frac{1}{2}$	0	0	0	0
$I_z$ – isospin $z$ -component	$-\frac{1}{2}$	$+\frac{1}{2}$	0	0	0	0
S - strangeness	0	0	-1	0	0	0
C - charm	0	0	0	+1	0	0
B – bottomness	0	0	0	0	-1	0
T - topness	0	0	0	0	0	+1

Table 15.1: Quark quantum numbers.

The hypercharge is defined as

$$Y = B + S - \frac{C - B + T}{3}$$
 (15.2)

Thus Y is equal to  $\frac{1}{3}$  for the u and d quarks,  $-\frac{2}{3}$  for the s quark, and 0 for all other quarks. More details and derivations on the quark structure of mesons and baryons can be found e.g. in Ref. [6].

The naming scheme for hadrons has been updated by the Particle Data Group in 2023, to include the heavy "exotic" states discovered recently, the tetraquark  $(qq\bar{q}\bar{q})$  and pentaquark  $(qqqq\bar{q})$  candidates (see "Naming Scheme for Hadrons" in this Review).

### 15.3 Mesons

Mesons have baryon number  $\mathcal{B} = 0$ . In the quark model, they are  $q\bar{q}'$  bound states of quarks q and antiquarks  $\bar{q}'$  (the flavors of q and q' may be different).

If the orbital angular momentum of the  $q\bar{q}'$  state is  $\ell$ , then the parity P is  $(-1)^{\ell+1}$ . The meson spin J is given by the usual relation  $|\ell-s| \leq J \leq |\ell+s|$ , where s=0 (antiparallel quark spins) or s=1 (parallel quark spins). The charge conjugation, or C-parity  $C=(-1)^{\ell+s}$ , is defined only for states made of quarks and their own antiquarks. The C-parity can be generalized to the G-parity  $G=(-1)^{I+\ell+s}$  for mesons made of quarks and their own antiquarks (isospin  $|I|_z=0$ ), and for the charged  $u\bar{d}$  and  $d\bar{u}$  states (isospin |I|=1).

The mesons are classified in  $J^{PC}$  multiplets. The  $\ell=0$  states are the pseudoscalars  $(0^{-+})$  and the vectors  $(1^{--})$ . The orbital excitations  $\ell=1$  are the scalars  $(0^{++})$ , the axial vectors  $(1^{++})$  and  $(1^{+-})$  aka pseudovectors, and the tensors  $(2^{++})$ . Assignments for many of the known mesons are given in Tables 15.2, 15.3 and 15.4. Radial excitations are denoted by the principal quantum number n. The very short lifetime of the t quark  $(\to W^+ b)$  makes it likely that bound-state hadrons containing t quarks and/or antiquarks do not exist.

States in the natural spin-parity series  $P=(-1)^J$  must, according to the above, have s=1 and hence, CP=+1. Thus, mesons with natural spin-parity and CP=-1 (0<sup>+-</sup>, 1<sup>-+</sup>, 2<sup>+-</sup>, 3<sup>-+</sup>, etc.) are forbidden in the  $q\bar{q}'$  model. The  $J^{PC}=0^{--}$  state is forbidden as well. Mesons with such exotic quantum numbers may exist, but would lie outside the  $q\bar{q}'$  model (see section 15.4 below on exotic mesons).

Following SU(3), the nine possible  $q\bar{q}'$  combinations containing the light u, d, and s quarks are grouped into an octet and a singlet of light quark mesons:

Table 15.2: Suggested  $q\bar{q}$  quark-model assignments for the lightest mesons made of u, d and s quarks. Mesons in boldface are included in the Summary Table. The wave functions f and f' are given in the text (Eq. (15.9)) and the singlet-octet mixing angles in Table 15.5 below for the well established nonets. The classification of the  $0^{++}$  mesons is controversial: (i) the scalars  $a_0(980)$ ,  $K_0^*(700)$ ,  $f_0(980)$  and  $f_0(500)$ , omitted from the table, are often considered to be four-quark states, but are also proposed for the ground state scalar nonet (see the chapter "Scalar Mesons below 1 GeV" in this Review); (ii) there are three isoscalar  $0^{++}$  mesons,  $f_0(1370)$ ,  $f_0(1500)$  and  $f_0(1710)$ , both  $f_0(1500)$  and  $f_0(1710)$  being proposed as glueballs. The three states are expected to mix. The isoscalar assignments in the  $2^1S_0$  ( $0^{-+}$ ) nonet are also tentative. Details and alternative schemes can be found in "Spectroscopy of Light Meson Resonances" in this Review.

- <sup>a</sup> The 1<sup>+±</sup> and 2<sup>-±</sup> isospin  $\frac{1}{2}$  states mix. In particular, the  $K_{1A}$  and  $K_{1B}$  are nearly equal mixtures of the  $K_1(1270)$  and  $K_1(1400)$  [7]. The 2<sup>-±</sup> mixed partner of the  $K_2(1770)$  is the established  $K_2(1820)$ .
- <sup>b</sup> The physical vector mesons are mixtures of  $1^3D_1$  and  $2^3S_1$  (for a discussion see [8]).
- <sup>c</sup> This state has also been proposed as a tetraquark state [9].
- <sup>d</sup> The  $\eta(1475)$  and  $\eta(1405)$  (not shown) may be manifestations of a single state [10].
- <sup>e</sup> This state has also been proposed as the ground state tensor glueball [11,12].

$n^{2s+1}\ell_J$	$J^{PC}$	I = 1	$I = \frac{1}{2}$	I = 0	I = 0
		$u\bar{d},  \bar{u}d,$	$u\bar{s}, d\bar{s};$	f'	f
		$\frac{1}{\sqrt{2}}(d\bar{d}-u\bar{u})$	$\bar{d}s,\bar{u}s$		
$-1^{1}S_{0}$	0-+	$\pi$	K	η	$\eta'(958)$
$1^{3}S_{1}$	1	ho(770)	$K^*(892)$	$\phi(1020)$	$\omega(782)$
$1^{3}P_{0}$	$0_{++}$	$a_0(1450)$	$K_0^*(1430)$	$f_0(1370, 1$	500, 1710)
$1^{1}P_{1}$	$1^{+-}$	$b_1(1235)$	$oldsymbol{K_{1B}}^{\mathrm{a}}$	$h_1(1415)$	$h_1(1170)$
$1^{3}P_{1}$	1++	$a_1(1260)$	$m{K_{1A}}^{ m a}$	$f_1(1420)$	$f_1(1285)$
$1^{3}P_{2}$	$2^{++}$	$a_2(1320)$	$K_2^st(1430)$	$f_2^{\prime}(1525)$	$f_2(1270)$
$1^{3}D_{1}$	1	ho(1700)	$\overline{K^*}(1680)^{ m b}$	$ar{\phi}(2170)^{ ext{c}}$	$\omega(1650)$
$1^{1}D_{2}$	$2^{-+}$	$\pi_2(1670)$	$K_2(1770)^{\mathrm{a}}$	$\eta_2(1870)$	$\eta_2(1645)$
$1^{3}D_{3}$	3	$ ho_3(1690)$	$K_3^*(1780)$	$\phi_3(1850)$	$\omega_3(1670)$
$1^{3}F_{4}$	$4^{++}$	$a_4(1970)$	$K_4^st(2045)$	$f_4(2300)$	$f_4(2050)$
$1^{3}G_{5}$	5	$\rho_5(2350)$	$K_5^*(2380)$		
$2^{1}S_{0}$	$0_{-+}$	$\pi(1300)$	K(1460)	$\eta(1475)^{ m d}$	$\eta(1295)$
$2^{3}S_{1}$	1	ho(1450)	$K^*(1410)^{ m b}$	$\phi(1680)$	$\omega(1420)$
$2^{3}P_{1}$	1++	$a_1(1640)$	$K_1(1650)$		
$2^{3}P_{2}$	$2^{++}$	$a_2(1700)$	$K_2^*(1980)$	$f_2(1950)^{ m e}$	$f_2(1640)$
$2^{1}D_{2}$	$2^{-+}$	$\pi_2(1880)$	_ '		
$3^1S_0$	0-+	$\pi(1800)$	K(1830)		$\eta(1760)$

**Table 15.3:**  $c\bar{c}$  quark-model assignments for the charmonium mesons with established  $J^{PC}$  and their corresponding open charm mesons. Mesons in boldface are included in the Meson Summary Table. The open flavor states in the  $1^{+-}$  and  $1^{++}$  rows are mixtures of the  $1^{+\pm}$  states.

<sup>&</sup>lt;sup>e</sup> The interpretation of this state as a single resonance is unclear due to substantial threshold effects in this energy region.

$\overline{n^{2s+1}\ell_J}$	$J^{PC}$	I = 0	$I = \frac{1}{2}$	I = 0
		$c\bar{c}$	$c\bar{u}, c\bar{d};$	$c \bar s;$
			$\bar{c}u,  \bar{c}d$	$ar{c}s$
$1^{1}S_{0}$	$0_{-+}$	$\eta_c(1S)$	D	$D_s^\pm$
$1^{3}S_{1}$	1	$J/\psi(1S)$	$D^*$	$D_s^{*\pm}$
$1^{3}P_{0}$	$0_{++}$	$\chi_{c0}(1P)$	$D_0^*(2300)^{\mathrm{a}}$	$D_{s0}^*(2317)^{\pm { m b}}$
$1  {}^{3}P_{1}$	$1^{++}$	$\chi_{c1}(1P)$	$D_1(2430)^{ m c}$	$D_{s1}(2460)^{\pm\mathrm{b}}$
$1  {}^{1}P_{1}$	$1^{+-}$	$h_c(1P)$	$D_1(2420)$	$D_{s1}(2536)^\pm$
$1{}^{3}P_{2}$	$2^{++}$	$\chi_{c2}(1P)$	$D_2^st(2460)$	$D_{s2}^*(2573)^\pm$
$2^{1}S_{0}$	$0_{-+}$	$\eta_c(2S)$	$D_0(2550)^0$	$D_{s0}(2590)^+$
$2^{3}S_1$	1	$\psi(2S)$	$D_1^*(2600)^0$	$D_{s1}^*(2700)^{\pm \mathrm{d}}$
$1^{3}D_{1}$	1	$\psi(3770)$	$D_1^*(2760)^0$	$D_{s1}^*(2860)^{\pm d}$
$1^{3}D_{2}$	$2^{}$	$\psi_2(3823)$	$D_2(2740)^0$	
$2^{3}P_{J}$	$0^{++}$	$\chi_{c0}(3860)$		
	$2^{++}$	$\chi_{c2}(3930)$	$D_2^*(3000)^0$	
$3{}^{3}S_{1}$	1	$\psi(4040)$		
$2^{3}D_{1}$	1	$\psi(4160)^{ m e}$		
$4^{3}S_{1}$	1	$\psi(4415)$		
$\frac{1^{3}D_{3}}{}$	3	$\psi_3(3842)$	$D_3^*(2750)$	$D_{s3}^*(2860)^\pm$

$$\mathbf{3} \otimes \overline{\mathbf{3}} = \mathbf{8} \oplus \mathbf{1} \ . \tag{15.3}$$

A fourth quark such as charm c can be included by extending SU(3) to SU(4). However, SU(4) is badly broken owing to the much heavier c quark. Nevertheless, in an SU(4) classification, the sixteen mesons are grouped into a 15-plet and a singlet:

$$\mathbf{4} \otimes \overline{\mathbf{4}} = \mathbf{15} \oplus \mathbf{1} . \tag{15.4}$$

The weight diagrams for the ground-state pseudoscalar  $(0^{-+})$  and vector  $(1^{--})$  mesons are depicted in Fig. 15.1. The light quark mesons are members of nonets building the middle plane in Fig. 15.1(a) and (b).

Isoscalar states with the same  $J^{PC}$  mix, but mixing between the two light quark isoscalar mesons, and the much heavier charmonium and bottomonium states, are generally assumed to be

<sup>&</sup>lt;sup>a</sup> In unitarized chiral perturbation theory this meson splits into two states at 2105 and 2451 MeV [1,13].

<sup>&</sup>lt;sup>b</sup> The masses are considerably smaller than most theoretical predictions. They have also been considered as tetraquark or  $D^{(*)}K$  molecular states.

<sup>&</sup>lt;sup>c</sup> This meson splits into two states at 2247 and 2555 MeV [1].

<sup>&</sup>lt;sup>d</sup> Mixtures of the  $1^3D_1$  and  $2^3S_1$  states.

Table 15.4:	$b\bar{b}$ qua	rk-model	assignments	for the	bottomonium	mesons
with establish	$\mathrm{ed}\ J^{PC}$	and their	r correspondi	ng oper	bottom meso	ns.

$n^{2s+1}\ell_J$	$J^{PC}$	I = 0	$I = \frac{1}{2}$	I = 0	I = 0
		$b ar{b}$	$b\bar{u},b\bar{d};$	$b\bar{s};$	$b\bar{c};$
			$\bar{b}u,\bar{b}d$	$ar{b}s$	$ar{b}c$
$1^{1}S_{0}$	0-+	$\eta_b(1S)$	B	$B_s^0$	$B_c^\pm$
$1{}^{3}S_{1}$	1	$\Upsilon(1S)$	$B^*$	$B_s^*$	
$1^{3}P_{0}$	$0^{++}$	$\chi_{b0}(1P)$			
$1{}^{3}P_{1}$	1++	$\chi_{b1}(1P)$			
$1  {}^{1}P_{1}$	1+-	$h_b(1P)$	$B_1(5721)$	$B_{s1}(5830)^0$	
$1{}^{3}P_{2}$	$2^{++}$	$\chi_{b2}(1P)$	$B_2^*(5747)$	$B_{s2}^*(5840)^0$	
$2^{1}S_{0}$	$0_{-+}$	$\eta_b(2S)$			$B_c(2S)^\pm$
$2{}^{3}S_{1}$	1	$\Upsilon(2S)$			
$1  {}^3D_2$	$2^{}$	$\Upsilon_2(1D)$			
$2^{3}P_{J}$	$0, 1, 2^{++}$	$\chi_{b0,1,2}(2P)$			
$2^{1}P_{1}$	1+-	$h_b(2P)$			
$3{}^{3}S_{1}$	1	$\Upsilon(3S)$			
$3^{3}P_{J}$	$0, 1, 2^{++}$	$\chi_{b1,2}(3P)$			
$\frac{4^{3}S_{1}}{}$	1	$\Upsilon(4S)$			

negligible. In the following, we shall use the generic names a for the I=1, K for the I=1/2, f and f' for the I=0 members of the light quark nonets. Thus, the physical isoscalars are mixtures of the SU(3) wave function  $\psi_8$  and  $\psi_1$ :

$$f' = \psi_8 \cos \theta - \psi_1 \sin \theta , \qquad (15.5)$$

$$f = \psi_8 \sin \theta + \psi_1 \cos \theta \,\,\,\,(15.6)$$

where  $\theta$  is the nonet mixing angle and

$$\psi_8 = \frac{1}{\sqrt{6}} (u\bar{u} + d\bar{d} - 2s\bar{s}) , \qquad (15.7)$$

$$\psi_1 = \frac{1}{\sqrt{3}} (u\bar{u} + d\bar{d} + s\bar{s}) \ . \tag{15.8}$$

The mixing relations are often rewritten to exhibit the  $u\bar{u}+d\bar{d}$  and  $s\bar{s}$  components which decouple for the "ideal" mixing angle  $\theta_i$ , such that  $\tan\theta_i=1/\sqrt{2}$  (or  $\theta_i=35.3^\circ$ ). Defining  $\alpha=\theta+54.7^\circ$ , one obtains the physical isoscalar state in the flavor basis

$$f' = \frac{1}{\sqrt{2}}(u\bar{u} + d\bar{d})\cos\alpha - s\bar{s}\sin\alpha , \qquad (15.9)$$

and its orthogonal partner f (replace  $\alpha$  by  $\alpha$  –90°). Thus for ideal mixing ( $\alpha_i = 90^\circ$ ), the f' becomes pure  $s\bar{s}$  and the f pure  $u\bar{u} + d\bar{d}$ . The mixing angle  $\theta$  can be derived by diagonalizing the mass matrix

$$\begin{pmatrix} m_8 & m_{81} \\ m_{18} & m_1 \end{pmatrix}. (15.10)$$

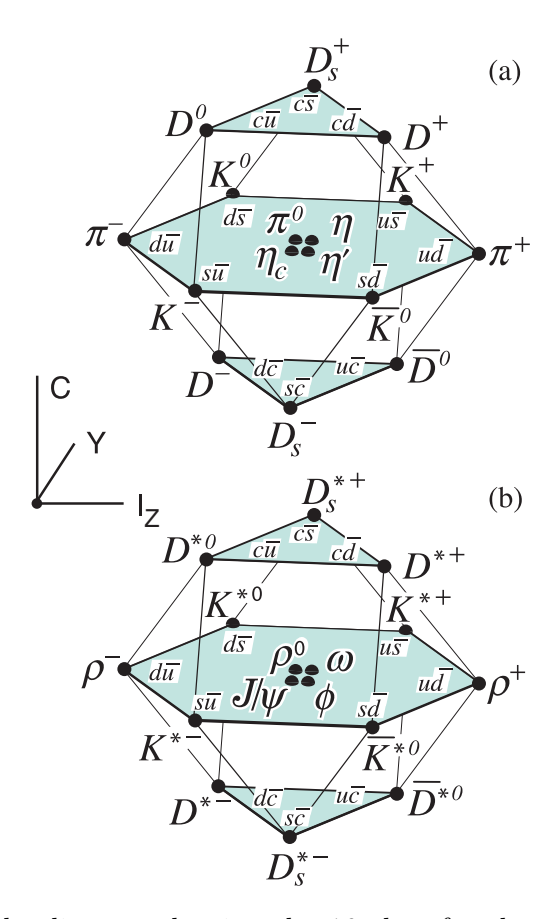


**Figure 15.1:** SU(4) weight diagram showing the 16-plets for the pseudoscalar (a) and vector mesons (b) made of the u, d, s, and c quarks as a function of isospin  $I_z$ , charm C, and hypercharge  $Y = \mathcal{B} + S - \frac{C}{3}$ . The nonets of light mesons occupy the central planes to which the  $c\bar{c}$  states have been added.

The mass eigenvalues are  $m_{f'}$  and  $m_f$ . The mixing angle is given by

$$\tan \theta = \frac{m_8 - m_{f'}}{m_{81}} \ . \tag{15.11}$$

Calculating  $m_8$  and  $m_{81}$  from the wave functions Eq. (15.7) and Eq. (15.8), and expressing the quark masses as a function of the I = 1/2 and I = 1 meson masses, one obtains

$$\tan \theta = \frac{4m_K - m_a - 3m_{f'}}{2\sqrt{2}(m_a - m_K)} , \qquad (15.12)$$

which also determines the sign of  $\theta$ . Alternatively, one can express the mixing angle as a function of all nonet masses. The octet mass is given by

$$m_8 = m_{f'}\cos^2\theta + m_f\sin^2\theta \tag{15.13}$$

whence

$$\tan^2 \theta = \frac{4m_K - m_a - 3m_{f'}}{-4m_K + m_a + 3m_f} \ . \tag{15.14}$$

Eliminating  $\theta$  from Eq. (15.12) and Eq. (15.14) leads to the sum rule [14]

$$(m_f + m_{f'})(4m_K - m_a) - 3m_f m_{f'} = 8m_K^2 - 8m_K m_a + 3m_a^2.$$
 (15.15)

This relation is verified for the ground-state vector mesons. We identify the  $\phi(1020)$  with the f' and the  $\omega(783)$  with the f. Thus

$$\phi(1020) = \psi_8 \cos \theta_V - \psi_1 \sin \theta_V , \qquad (15.16)$$

$$\omega(782) = \psi_8 \sin \theta_V + \psi_1 \cos \theta_V , \qquad (15.17)$$

with the vector mixing angle  $\theta_V = 36.5^{\circ}$  from Eq. (15.14), very close to ideal mixing. Thus  $\phi(1020)$  is nearly pure  $s\bar{s}$ . For ideal mixing, Eq. (15.12) and Eq. (15.14) lead to the relations

$$m_K = \frac{m_f + m_{f'}}{2} , \quad m_a = m_f ,$$
 (15.18)

which are satisfied for the vector mesons.

The situation for the pseudoscalar and scalar mesons is not so clear cut, either theoretically or experimentally. For the pseudoscalars, the mixing angle is small. This can be understood qualitatively via gluon-line counting of the mixing process. The size of the mixing process between the nonstrange and strange mass bases scales as  $\alpha_s^2$ , not  $\alpha_s^3$ , because of two rather than three gluon exchange as it does for the vector mesons. It may also be that the lightest isoscalar pseudoscalars mix more strongly with excited states or with states of substantial non- $\bar{q}q$  content, as will be discussed below.

In fact a large mixing from hadronic loops is expected for scalar mesons, no matter what model is assumed for  $q\bar{q}$  pair production [15]. A variety of analysis methods lead to similar results: First, for these states, Eq. (15.15) is satisfied only approximately. Then Eq. (15.12) and Eq. (15.14) lead to somewhat different values for the mixing angle. Identifying the  $\eta$  with the f' one gets

$$\eta = \psi_8 \cos \theta_P - \psi_1 \sin \theta_P \,, \tag{15.19}$$

$$\eta' = \psi_8 \sin \theta_P + \psi_1 \cos \theta_P \ . \tag{15.20}$$

Following chiral perturbation theory, the meson masses in the mass formulae (Eq. (15.12) and Eq. (15.14)) might be replaced by their squares. Table 15.5 lists the mixing angle  $\theta_{\text{lin}}$  from Eq. (15.14) (using the neutral members of the nonets) and the corresponding  $\theta_{\text{quad}}$  obtained by replacing the meson masses by their squares throughout. The mixing angles in the 1<sup>--</sup>, 2<sup>++</sup> and 3<sup>--</sup> nonets are not far from ideal, while larger  $s\bar{s}$ -( $u\bar{u}+d\bar{d}$ ) mixing is predicted from hadronic loops in the 0<sup>++</sup>, 0<sup>-+</sup> and 1<sup>+±</sup> nonets [15].

**Table 15.5:** Singlet-octet mixing angles for the well established nonets from the linear mass formula Eq. (15.14) and its quadratic version in which the masses are squared. The 1<sup>++</sup> and 1<sup>+-</sup> nonet mixing angles depend on the mixing angle  $\theta_{K_1}$  between  $K_{1A}$  and  $K_{1B}$ . The recommended values are  $\sim 23^{\circ}$  and  $\sim 28^{\circ}$  for 1<sup>++</sup> and 1<sup>+-</sup>, respectively, with  $\theta_{K_1} \sim 35^{\circ}$  [7].

$n^{2s+1}\ell_J$	$J^{PC}$	$\theta_{ m quad}$	$\theta_{ m lin}$
		[°]	[°]
$1^{1}S_{0}$	$0_{-+}$	-11.3	-24.5
$1^{3}S_{1}$	1	39.2	36.5
$1^{3}P_{2}$	$2^{++}$	29.6	28.0
$1^{3}D_{3}$	3	31.8	30.8

The pseudoscalar mixing angle  $\theta_P$  can also be measured by comparing the partial widths for radiative  $J/\psi$  decay into a vector and a pseudoscalar [16], radiative  $\phi(1020)$  decay into  $\eta$  and  $\eta'$  [17],

radiative decays between pseudoscalar and vector mesons [18], or  $\bar{p}p$  annihilation at rest into a pair of vector and pseudoscalar or into two pseudoscalars [19,20]. One obtains a mixing angle between  $-10^{\circ}$  and  $-20^{\circ}$ . More recently, a lattice QCD simulation, Ref. [21], has successfully reproduced the masses of the  $\eta$  and  $\eta'$ , and as a byproduct find a mixing angle  $\theta_{lin} = -14.1(2.8)^{\circ}$ . We return to this point in Sec. 15.8.

The nonet mixing angles can be measured in  $\gamma\gamma$  collisions, e.g., for the  $0^{-+}$ ,  $0^{++}$ , and  $2^{++}$  nonets. In the quark model, the amplitude for the coupling of neutral mesons to two photons is proportional to  $\sum_{i} Q_i^2$ , where  $Q_i$  is the charge of the *i*-th quark. The  $2\gamma$  partial width of an isoscalar meson with mass m is then given in terms of the mixing angle  $\alpha$  by

$$\Gamma_{2\gamma} = C(5\cos\alpha - \sqrt{2}\sin\alpha)^2 m^3 , \qquad (15.21)$$

for f' and f ( $\alpha \to \alpha - 90^{\circ}$ ). The coupling C may depend on the meson mass. It is often assumed to be a constant in the nonet. For the isovector a, one finds  $\Gamma_{2\gamma} = 9 \, C \, m^3$ . Thus the members of an ideally mixed nonet couple to  $2\gamma$  with partial widths in the ratios f: f': a = 25: 2: 9. For tensor mesons, one finds from the ratios of the measured  $2\gamma$  partial widths for the  $f_2(1270)$  and  $f'_2(1525)$  mesons a mixing angle  $\alpha_T$  of  $(81\pm 1)^{\circ}$ , or  $\theta_T = (27\pm 1)^{\circ}$ , in accord with the linear mass formula. For the pseudoscalars, one finds from the ratios of partial widths  $\Gamma(\eta' \to 2\gamma)/\Gamma(\eta \to 2\gamma)$  a mixing angle  $\theta_P = (-18 \pm 2)^{\circ}$ , while the ratio  $\Gamma(\eta' \to 2\gamma)/\Gamma(\pi^0 \to 2\gamma)$  leads to  $\sim -24 \, ^{\circ}$ . SU(3) breaking effects for pseudoscalars are discussed in [22].

The partial width  $\Gamma$  for the decay of a scalar or a tensor meson into a pair of pseudoscalar mesons is model-dependent. Following Ref. [23],

$$\Gamma = C \times \gamma^2 \times |F(q)|^2 \times q , \qquad (15.22)$$

where C is a nonet constant, q the momentum of the decay products, F(q) a form factor, and  $\gamma^2$  the SU(3) coupling. Details and explicit expressions for  $\gamma^2$  and F(q) are given in "Spectroscopy of Light Meson Resonances". The decay of a  $q\bar{q}$  meson into a pair of mesons involves the creation of a  $q\bar{q}$  pair, and SU(3) symmetry assumes that the matrix elements for the creation of  $s\bar{s}$ ,  $u\bar{u}$ , and  $d\bar{d}$  pairs are equal. An excellent fit to the tensor meson decay widths is obtained assuming SU(3) symmetry and a pseudoscalar mixing angle  $\theta_P \simeq -17$  ° [23].

The analysis of resonances is complicated by the presence of thresholds such as  $K\bar{K}$  in  $a_0(980) \to \eta\pi$  or  $f_0(980) \to \pi\pi$ , which affect the resonance masses and widths. A particularly nasty kinematic effect is the triangle singularity in which one of the primary decay daughters in turn decays and is emitted backwards, catching up and scattering with the second primary product. This mechanism generates fake peaks in the final state and has been proposed as alternative explanation for several meson (and baryon) signals. Prominent examples are the  $\eta(1475) \to K^*(\to K\pi)\bar{K}$  and  $\eta(1410) \to a_0(980)(\to \eta\pi)\pi$  signals which could be due to one single state [10] (as shown in Table 15.2).

Furthermore, to parametrize resonances, many data analyses resort to Breit-Wigner amplitudes which are not suitable to describe broad interfering mesons with the same quantum numbers, as they violate unitarity. This is in particular the case in the mass range above 1500 MeV where radial and orbital excitations, e.g. of broad scalar and tensor mesons, start to accumulate. A better approach is to determine the T-matrix poles in the complex plane, where resonances are usually located on the second Riemann sheet.

# 15.4 Exotic mesons

There are two classes of colorless exotic mesons allowed in QCD: multiquark states (section 15.4.1) and mesons with active gluons, bound states of gluons (the glueballs, section 15.4.2) and  $q\bar{q}$  states with "valence" gluons (the hybrids, section 15.4.3). The first class contains the simplest

system consisting of two quarks and two antiquarks (tetraquarks). Compact tetraquarks (also called "diquonium" in the older literature) are made of diquarks and antidiquarks. Hadroquarkonia consist of a pair of heavy quark and antiquark in a compact core surrounded by a light-quark cloud. In hadronic "molecules" the building blocks are color-neutral hadrons bound by meson exchanges.

#### 15.4.1 Tetraquarks

The existence of a light nonet composed of four quarks (tetraquarks) with masses below 1 GeV was suggested a long time ago [24,25]. Coupling two triplets of light quarks u, d, and s, one obtains nine states, of which the six symmetric (uu, dd, ss, ud + du, us + su, ds + sd) form the six dimensional representation  $\bf 6$ , while the three antisymmetric (ud - du, us - su, ds - sd) form the three dimensional representation  $\bf 3$  of SU(3):

$$\mathbf{3} \otimes \mathbf{3} = \mathbf{6} \oplus \mathbf{\bar{3}} \ . \tag{15.23}$$

Hence for tetraquarks one gets the reduction

$$3 \otimes 3 \otimes \overline{3} \otimes \overline{3} 
= 6 \oplus \overline{3} \otimes \overline{6} \otimes 3 
= \overline{3} \otimes 3 \oplus 6 \otimes \overline{6} \oplus 6 \otimes 3 \oplus \overline{3} \otimes \overline{6} 
= 9 \oplus 36 \oplus 18 \oplus \overline{18}.$$
(15.24)

Combining with spin and color and requiring antisymmetry for diquarks and antidiquarks, one finds for ground states (zero angular momenta) that the most deeply bound tetraquarks (and hence the lightest ones) form a nonet and are scalar mesons (see also [6]). The masses are estimated to be below 900 MeV. The strange quark determines the mass splittings and one obtains a mass inverted spectrum with a light isosinglet  $(f_0(500))$ , a medium heavy isodoublet  $(K_0^*(700))$  and a heavy isotriplet  $(a_0(980))$  + isosinglet  $(f_0(980))$ . In alternative schemes these states build the lightest  $q\bar{q}$  scalar nonet (for details see "Scalar mesons below 1 GeV" in this Review).

A plethora of new heavy multiquark candidates have been reported in the charmonium spectrum (Fig. 15.2). Details and references can be found in the review "Heavy non- $q\bar{q}$  Mesons", see also Refs. [26–29].

The most prominent one is the  $\chi_{c1}(3872)$  (was X(3872)), first observed by BELLE in 2003 in B-decays in the final state  $J/\psi \pi^+\pi^-$  [30] and firmly established by many experiments (Babar, BESIII, CDF, D0, LHCb) in several production modes  $(e^+e^-, \Lambda_b \text{ decay}, \bar{p}p, pp)$ . This narrow state (< 1 MeV) decays mainly into  $D^0\bar{D}^{0*}$  and is right at the  $D^0\bar{D}^{0*}$  threshold. Its composition is believed to be mostly molecular, bound by pion exchange. Its existence was already predicted in 1991 [31]. Many non- $c\bar{c}$  candidates have been reported since then above the open charm threshold, with quantum numbers compatible with  $c\bar{c}$ , but which are not expected in the pure charmonium spectrum. In addition, one observes isovector (charged) mesons decaying into  $c\bar{c}$  states plus a charged pion or kaon. (They are listed in this Review under "Other mesons".) For example, the  $1^{+-}$   $T_{c\bar{c}1}(3900)^+$  (was  $Z_c(3900)^+$ ) and  $T_{c\bar{c}s1}(4000)^+$  (was  $Z_{cs}(4000)^-$ ) cannot be pure charmonia, but are compatible with  $c\bar{c}u\bar{d}$  and  $c\bar{c}s\bar{u}$ , respectively. They could belong to the same nonet, hence identifying the other multiplet members might shed light on the structure of such states.

Even more remarkable are the observations by LHCb of a doubly charmed state  $T_{cc}(3875)^+$   $(cc\bar{u}\bar{d})$  [32] at the  $D_0D_0^*$  threshold and of a  $T_{cc\bar{c}\bar{c}}(6900)$  [33] decaying into a pair of  $J/\psi(1S)$ . Similar states begin to emerge also in the bottomonium spectrum, such as the  $1^{+-}$   $T_{b\bar{b}1}(10610)^+$  (was  $Z_b(10610)^+$ ) and  $T_{b\bar{b}1}(10650)^+$  (was  $Z_b(10650)^+$ ), both  $b\bar{b}u\bar{d}$ . Many of these states may be hadronic modules made of charge conjugated pairs of mesons such as  $D^{(*)}$ ,  $D_s^{(*)}$  or their excitations, and their B and  $B^*$  counterparts. They could also be mimicked by kinematical effects such as triangle singularities.

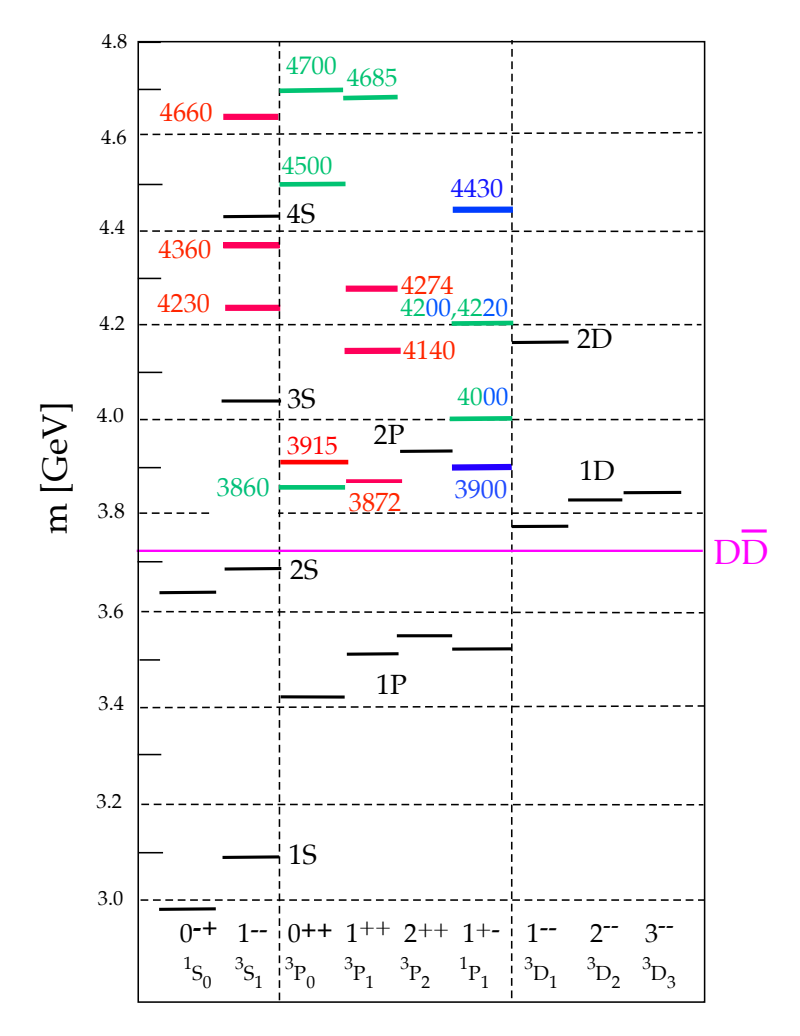


Figure 15.2: Mass spectrum with known  $I^G(J^{PC})$  observed in the charmonium region. The  $D\bar{D}$  line shows the open charm threshold. The well-known  $c\bar{c}$  mesons are shown in black. (The  $1^1D_2$   $\eta_{c2}$ , expected around 3800 MeV, has not been seen yet.) The established additional observed states are shown in red, and the states needing confirmation (i.e. omitted from the Summary Tables) are labeled in green. The blue color denotes exotic isovectors.

#### 15.4.2 Glueballs

QCD predicts the existence of extra isoscalar mesons which cannot be addressed by the quark model. In the pure gauge theory they contain only gluons. The ground state glueball is predicted by lattice gauge theories to be 0<sup>++</sup>, the first excited state 2<sup>++</sup>. Errors on the mass predictions are large. From Ref. [34] one obtains 1750 (50) (80) MeV for the mass of the lightest 0<sup>++</sup> glueball from quenched QCD. As an example for the glueball mass spectrum, we show in Fig. 15.3 a calculation from [35]. A mass of 1710 MeV is predicted for the ground state, also with an error of about 100 MeV. Earlier work by other groups produced masses at 1650 MeV [36] and 1550 MeV [37] (see also [38].

These calculations are made in the so-called "quenched approximation" which neglects  $q\bar{q}$  loops. However, both glue and  $q\bar{q}$  states couple to singlet scalar mesons. Therefore glueballs will mix with nearby  $q\bar{q}$  states of the same quantum numbers. The first results from lattice calculations, which include these effects, indicate that the mass shifts are small. We return to a discussion of this

point in Sec. 15.8, see also Fig. 15.15. The most recent prediction [39] quotes the more precise masses  $1653 \pm 26$ ,  $2376 \pm 32$  and  $2561 \pm 40$  MeV for the  $0^{++}$ ,  $2^{++}$  and  $0^{-+}$  respectively. Heavier glueballs with quantum numbers  $0^{-+}$ ,  $2^{-+}$ ,  $1^{+-}$ , etc. are predicted above 2500 MeV and the lowest exotic ones (with exotic quantum numbers such as  $0^{+-}$  and  $2^{+-}$ ) are expected above 4000 MeV (Fig. 15.3). In holographic QCD the  $0^{-+}$  is predicted to be very broad [40] and the  $1^{+-}$  is at least as broad as its mass [41]. Calculations of the three lowest scalar and pseudoscalar glueballs masses in pure Yang-Mills theory are in quantitative agreement with lattice results [42].

The existence of three singlet scalar mesons around 1.5 GeV suggests additional degrees of freedom such as glue, since only two mesons are predicted in this mass range (as indicated in Table 15.2). The  $f_0(1500)$  [23, 43] or, alternatively, the  $f_0(1710)$  [36], have been proposed as candidates for the scalar glueball, both states having considerable mixing also with the  $f_0(1370)$ . Following Ref. [44] the glue is distributed among the  $0^{++}$  isoscalars  $q\bar{q}$  mesons around 2 GeV. Other mixing schemes, in particular with the  $f_0(500)$  and the  $f_0(980)$ , have also been proposed [45]. According to a holographic model of low-energy QCD scalar glueballs decay strongly into kaons and  $\eta$  mesons, in good agreement with data on the  $f_0(1710)$  [46]. Details can be found in the review "Spectroscopy of Light Meson Resonances" and in Ref. [47]. See also the review "Scalar Mesons below 1 GeV" in this Review.

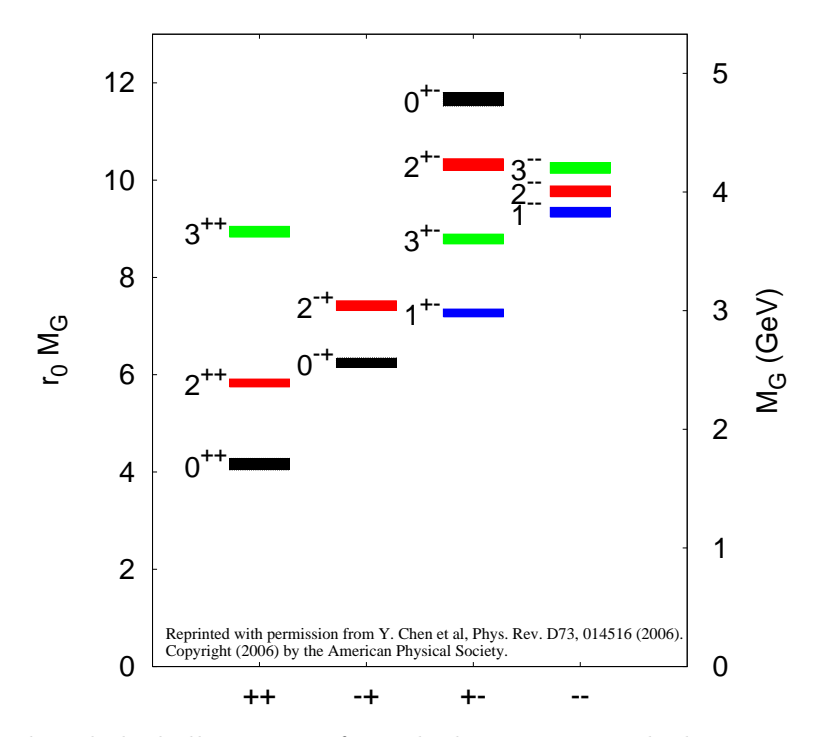


Figure 15.3: Predicted glueball spectrum from the lattice in quenched approximation (from [35]).

### 15.4.3 Hybrids

Mesons made of  $q\bar{q}$  pairs bound by excited gluons  $(q\bar{q}g)$  are also predicted. Early model estimates placed them in the 1.9 GeV mass region, according to gluon flux tube models [48]. In the bag model there are four nonets, among them an exotic  $1^{-+}$ , around or above 1.4 GeV [49, 50].

Lattice QCD calculations show that the lightest hybrid is an exotic  $1^{-+}$  state, at a mass around 2 GeV [51–53]. Fig. 15.13 will show an example of the spectroscopy from one group's [53] simulation.

There are so far two candidates for exotic states with quantum numbers  $1^{-+}$ , the  $\pi_1(1400)$  and  $\pi_1(1600)$ , which could be hybrids or four-quark states. However, a recent combined re-analysis of

 $\pi_1$  production in diffractive  $\pi^- p$  interaction and low energy  $\bar{p}p$  annihilation leads to a single pole at ~1560 MeV with a width of ~390 MeV, although a two-pole scenario cannot be excluded [54]. Recently BESIII has reported evidence for the existence of a  $1^{-+}$   $\eta_1(1855) \to \eta \eta'$  [55] which could be one of the isoscalar partners of the  $\pi_1(1600)$  in the  $1^{-+}$  hybrid nonet [56]. (For details and references, see the review "Spectroscopy of Light Meson Resonances" in this *Review*.)

#### 15.5 Baryons: qqq states

Baryons are fermions with baryon number  $\mathcal{B}=1$ , i.e., in the most general case, they are composed of three quarks plus any number of quark - antiquark pairs. Until recently, all established baryons were consistent with 3-quark (qqq) configurations, which we mainly discuss in this section. However, in 2015 the LHCb collaboration published first evidence for charmed 'pentaquark' states of minimal quark content  $c\bar{c}uud$  at invariant masses close to 4.4 GeV [57]. More refined LHCb [58] and D0 [59] experiments have revealed evidence for six such states called  $P_{c\bar{c}}(4312)^+$ ,  $P_{c\bar{c}s}(4338)^0$ ,  $P_{c\bar{c}}(4380)^+$ ,  $P_{c\bar{c}}(4440)^+$ ,  $P_{c\bar{c}}(4457)^+$ , and  $P_{c\bar{c}}(4459)^0$ . These states are located close to the thresholds of the production of ordinary baryon-meson pairs like  $\Sigma_c^+\bar{D}^0$  and  $\Sigma_c^+\bar{D}^{*0}$  and are consistent with the predictions in terms of molecular-like states [60,61]. A nice overview on the discussion of pentaquark and tetraquark states is given in Ref. [62]. See also the article on "Pentaquarks" in this Review.

The color part of the baryon wave function is an SU(3) singlet, a completely antisymmetric state of the three colors. Since the quarks are fermions, the wave function must be antisymmetric under interchange of any two equal-mass quarks (up and down quarks in the limit of isospin symmetry). Thus, it can be written as

$$|qqq\rangle_A = |\operatorname{color}\rangle_A \times |\operatorname{space}, \operatorname{spin}, \operatorname{flavor}\rangle_S,$$
 (15.25)

where the subscripts S and A indicate symmetry or antisymmetry under interchange of any two equal-mass quarks. Note the contrast with the state function for the three nucleons in  ${}^{3}$ H or  ${}^{3}$ He:

$$|NNN\rangle_A = |\operatorname{space}, \operatorname{spin}, \operatorname{isospin}\rangle_A.$$
 (15.26)

This difference has major implications for the internal structure, magnetic moments, etc. (For a nice discussion, see [63].)

#### 15.5.1 Light baryons

The "ordinary" light-flavor baryons are made up of u, d, and s quarks. The three flavors imply an approximate SU(3) flavor symmetry, which requires that baryons made of these quarks belong to the multiplets on the right side of

$$\mathbf{3} \otimes \mathbf{3} \otimes \mathbf{3} = \mathbf{10}_S \oplus \mathbf{8}_M \oplus \mathbf{8}_M \oplus \mathbf{1}_A \tag{15.27}$$

(see the section on "SU(n) Multiplets and Young Diagrams" in this Review). Here the subscripts indicate symmetric, mixed-symmetry, or antisymmetric states under interchange of any two quarks. The 1 is a  $|uds\rangle$  singlet state ( $\Lambda_1$ ), and the octet contains a similar state ( $\Lambda_8$ ). If these have the same spin and parity, they can mix. The mechanism is the same as for the mesons (see above). In the ground state multiplet, the SU(3) flavor singlet  $\Lambda_1$  is forbidden by Fermi statistics. The section on "SU(3) Isoscalar Factors and Representation Matrices," shows how relative decay rates in, say,  $10 \to 8 \otimes 8$  decays may be calculated.

For the light-flavor baryons (no c or b quark), flavor and spin may be combined in an approximate flavor-spin SU(6), in which the six basic states are  $d \uparrow, d \downarrow, \dots, s \downarrow (\uparrow, \downarrow = \text{spin up, down})$ . Then the baryons belong to the multiplets on the right side of

$$\mathbf{6} \otimes \mathbf{6} \otimes \mathbf{6} = \mathbf{56}_S \oplus \mathbf{70}_M \oplus \mathbf{70}_M \oplus \mathbf{20}_A. \tag{15.28}$$

These SU(6) multiplets decompose into flavor SU(3) multiplets as follows:

$$\mathbf{56} = {}^{4}\mathbf{10} \oplus {}^{2}\mathbf{8} \tag{15.29a}$$

$$70 = {}^{2}10 \oplus {}^{4}8 \oplus {}^{2}8 \oplus {}^{2}1 \tag{15.29b}$$

$$20 = {}^{2}8 \oplus {}^{4}1, \tag{15.29c}$$

where the superscript (2S+1) gives the net spin S of the quarks for each particle in the SU(3) multiplet. The  $J^P=1/2^+$  octet containing the nucleon and the  $J^P=3/2^+$  decuplet containing the  $\Delta(1232)$  together make up the "ground-state" 56-plet, in which the orbital angular momenta between the quark pairs are zero (so that the spatial part of the state function is trivially symmetric). The **70** and **20** require some excitation of the spatial part of the wave function in order to make the overall wave function symmetric. States with nonzero orbital angular momenta are classified in  $SU(6)\otimes O(3)$  supermultiplets.

It is useful to classify the baryons into bands that have the same number N of quanta of excitation. Each band consists of a number of supermultiplets, specified by  $(D, L_N^P)$ , where D is the dimensionality of the SU(6) representation, L is the total quark orbital angular momentum, and P is the total parity. Supermultiplets contained in bands up to N = 12 are given in [64]. The N = 0 band (with positive parity), which contains the nucleon and  $\Delta(1232)$ , consists only of the  $(56,0_0^+)$  supermultiplet. The N = 1 band (with negative parity) consists only of the  $(70,1_1^-)$  multiplet and contains the negative-parity baryons with masses below about 1.9 GeV. The N = 2 band (with positive parity) contains five supermultiplets:  $(56,0_2^+)$ ,  $(70,0_2^+)$ ,  $(56,2_2^+)$ ,  $(70,2_2^+)$ , and  $(20,1_2^+)$ , where the  $(56,0_0^+)$  represents the multiplet that contains the first radial excitations having the same quantum numbers as the ground state.

The wave functions of the non-strange baryons in the harmonic oscillator basis are often labeled by  $|X^{2S+1}L_{\pi}J^{P}\rangle$ , where S, L, J, P are as above, X = N or  $\Delta$ , and  $\pi = S, M$  or A denotes the symmetry of the spatial wave function. The possible model states for the bands with N=0,1,2 are given in Table 15.7. The assignment of experimentally observed states is only complete and well established up to the N=1 band. Some more tentative assignments for higher multiplets are suggested in [65].

In Table 15.6, quark-model assignments are given for many of the established baryons whose  $SU(6)\otimes O(3)$  compositions are relatively unmixed. Apart from the mixing of the  $\Lambda$  singlet and octet states, one must, however, keep in mind that states with same  $J^P$  but different L,S combinations can also mix. In the quark model with one-gluon exchange motivated interactions, the size of the mixing is determined by the relative strength of the tensor term with respect to the contact term (see below). The mixing is more important for the decay patterns of the states than for their positions. An example are the lowest lying  $(70,1_1^-)$  states with  $J^P=1/2^-$  and  $3/2^-$ . The physical states are

$$|N(1535)1/2^{-}\rangle = \cos(\Theta_S)|N^2P_M1/2^{-}\rangle - \sin(\Theta_S)|N^4P_M1/2^{-}\rangle$$
 (15.30)

$$|N(1520)3/2^{-}\rangle = \cos(\Theta_D)|N^2P_M3/2^{-}\rangle - \sin(\Theta)_D|N^4P_M3/2^{-}\rangle$$
 (15.31)

and the orthogonal combinations for  $N(1650)1/2^-$  and  $N(1700)3/2^-$ . The mixing is large for the  $J^P=1/2^-$  states ( $\Theta_S \approx -32^o$ ), but small for the  $J^P=3/2^-$  states ( $\Theta_D \approx +6^o$ ) [67–69].

All baryons of the ground state multiplets are known. Many of their properties, in particular their masses, are in good agreement with even the most basic versions of the quark model, including harmonic (or linear) confinement and a spin-spin interaction, which is responsible for the octet-decuplet mass shifts. A consistent description of the ground-state electroweak properties, however, requires refined relativistic constituent quark models.

**Table 15.6:** Quark-model assignments for some of the known baryons in terms of a flavor-spin SU(6) basis. Only the dominant representation is listed. Assignments for several states, especially for the  $\Lambda(1810)$ ,  $\Lambda(2350)$ ,  $\Xi(1620)$ ,  $\Xi(1690)$ ,  $\Xi(1820)$ , and  $\Xi(2030)$ , are merely educated guesses. 

† suggestions for assignments and re-assignments from Ref. [66].

$J^P$	$(D, L_N^P)$	S			nembers		Singlets
$1/2^{+}$	$(56,0_0^+)$	1/2	N(939)	$\Lambda(1116)$	$\Sigma(1193)$	$\Xi(1318)$	
$1/2^{+}$	$(56,0_2^+)$	1/2	N(1440)	$\Lambda(1600)$	$\Sigma(1660)$		
$1/2^{-}$	$(70,1_1^-)$	1/2	N(1535)	$\Lambda(1670)$	$\Sigma(1620)$	$\Xi(1620)$	$\Lambda(1405)$
					$\Sigma(1560)^{\dagger}$		
$3/2^{-}$	$(70,1_1^-)$	1/2	N(1520)	$\Lambda(1690)$	$\Sigma(1670)$	$\Xi(1820)$	$\Lambda(1520)$
$1/2^{-}$	$(70,1_1^-)$	3/2	N(1650)	$\Lambda(1800)$	$\Sigma(1750)$	$\Xi(1690)$	
					$\Sigma(1620)^{\dagger}$		
$3/2^{-}$	$(70,1_1^-)$	3/2	N(1700)	$\Lambda(?)$	$\Sigma(1940)^{\dagger}$	$\Xi(?)$	
$5/2^{-}$	$(70,1_1^-)$	3/2	N(1675)	$\Lambda(1830)$	$\Sigma(1775)$	$\Xi(1950)^{\dagger}$	
$1/2^{+}$	$(70,0_2^+)$	1/2	N(1710)	$\Lambda(1810)$	$\Sigma(1880)$	$\Xi(?)$	$\Lambda(1810)^{\dagger}$
$3/2^{+}$	$(56,2^{+}_{2})$	1/2	N(1720)	$\Lambda(1890)$	$\Sigma(?)$	$\Xi(?)$	
$5/2^{+}$	$(56,2^{\frac{1}{2}})$	1/2	N(1680)	$\Lambda(1820)$	$\Sigma(1915)$	$\Xi(2030)$	
$7/2^{-}$	$(70,3^{-}_{3})$	1/2	N(2190)	$\Lambda(?)$	$\Sigma(?)$	$\Xi(?)$	$\Lambda(2100)$
$9/2^{-}$	$(70,3^{-}_{3})$	3/2	N(2250)	$\Lambda(?)$	$\Sigma(?)$	$\Xi(?)$	
$9/2^{+}$	$(56,4_4^+)$	1/2	N(2220)	$\Lambda(2350)$	$\Sigma(?)$	$\Xi(?)$	
				Decuplet	members		
$3/2^{+}$	$(56,0_0^+)$	3/2	$\Delta(1232)$	$\Sigma(1385)$	$\Xi(1530)$	$\Omega(1672)$	
$3/2^{+}$	$(56,0^{+}_{2})$	3/2	$\Delta(1600)$	$\Sigma(1690)^{\dagger}$	$\Xi(?)$	$\Omega(?)$	
$1/2^{-}$	$(70,1_1^{-})$	1/2	$\Delta(1620)$	$\Sigma(1750)^{\dagger}$	$\Xi(?)$	$\Omega(?)$	
$3/2^{-}$	$(70,1_1^-)$	1/2	$\Delta(1700)$	$\Sigma(?)$	$\Xi(?)$	$\Omega(2012)$	
$5/2^{+}$		3/2	$\Delta(1905)$	$\Sigma(?)$	$\Xi(?)$	$\Omega(?)$	
$7/2^{+}$	$(56,2^{+}_{2})$	3/2	$\Delta(1950)$	$\Sigma(2030)$		$\Omega(?)$	
$11/2^{+}$	$(56,4_4^+)$		$\Delta(2420)$		Ξ(?)	$\Omega(?)$	

The situation for the excited states is much less clear. The assignment of some experimentally observed states with strange quarks to model configurations is only tentative and in many cases candidates are completely missing. Melde, Plessas and Sengl [66] have calculated baryon properties in relativistic constituent quark models, using one-gluon exchange and Goldstone-boson exchange for the modeling of the hyperfine interactions (see Sec. 15.7 on Dynamics). Both types of models give qualitatively comparable results and in geneeral, underestimate experimentally observed decay widths. Nevertheless, in particular on the basis of the observed decay patterns, the authors have assigned some additional states with strangeness to the SU(3) multiplets and suggest re-assignments for a few others. Among the new assignments are states with weak experimental evidence (two or three star ratings) and partly without firm spin/parity assignments, so that further experimental efforts are necessary before final conclusions can be drawn. We have added their suggestions in Table 15.6.

In the non-strange sector there are two main problems which are illustrated in Fig. 15.4, where the experimentally observed excitation spectrum of the nucleon (N and  $\Delta$  resonances) is compared to the results of a typical quark model calculation [70]. The lowest states from the N=2 band, the  $N(1440)1/2^+$ , and the  $\Delta(1600)3/2^+$ , appear lower than the negative parity states from the N=1 band (see Table 15.7) and much lower than predicted by most models. Also negative parity  $\Delta$  states from the N=3 band ( $\Delta(1900)1/2^-$ ,  $\Delta(1940)3/2^-$ , and  $\Delta(1930)5/2-$ ) are too low in energy. The low lying states show a clustering in groups of levels around 1700 MeV and 1900 MeV for  $N^*$ 

**Table 15.7:** N and  $\Delta$  states in the N=0,1,2 harmonic oscillator bands.  $L^P$  denotes angular momentum and parity, S the three-quark spin and 'sym'=A,S,M the symmetry of the spatial wave function. Listed are all possible spin/parity combinations and assignments of experimentally observed states. Only dominant components are indicated. Assignments in the N=2 band are partly tentative.

$\overline{N}$	sym	$L^P$	$\overline{S}$		N(I =	= 1/2)	
2	A	1+	1/2	1/2+	3/2+	-	-
2	M	$2^{+}$	3/2	$1/2^{+}$	$3/2^{+}$	$5/2^{+}$	$7/2^{+}$
2	M	$2^{+}$	1/2	-	$3/2^{+}$	$5/2^{+}$	-
2	M	0+	3/2	-	$3/2^{+}$	-	-
2	M	$0_{+}$	1/2	$1/2^+ N(1710)$	-	-	-
2	$\mathbf{S}$	$2^{+}$	3/2	-	-	-	-
2	$\mathbf{S}$	$2^{+}$	1/2	-	$3/2^+ N(1720)$	$5/2^+ N(1680)$	-
2	$\mathbf{S}$	$0_{+}$	3/2	-	-	-	-
2	$\mathbf{S}$	$0_{+}$	1/2	$1/2^+ N(1440)$	-	-	-
1	Μ	1-	3/2	$1/2^- N(1650)$	$3/2^- N(1700)$	$5/2^- N(1675)$	-
1	Μ	$1^{-}$	1/2	$1/2^- N(1535)$	$3/2^- N(1520)$	-	-
0	S	$0_{+}$	3/2	-	-	-	-
0	S	$0_{+}$	1/2	$1/2^+ N(938)$	-	-	_
N	sym		S		$\Delta(I =$	= 3/2)	
$\overline{2}$	A	1+	1/2	-	-	-	-
2	M	$2^{+}$	3/2	-	-	-	-
2	M	$2^{+}$	1/2	-	$3/2^{+}$	$5/2^{+}$	-
2	M	0+	3/2	-	-	-	-
2	M	0+	1/2	$1/2^+ \Delta(1750)$	-	-	-
2	$\mathbf{S}$	$2^{+}$	3/2	$1/2^+ \Delta(1910)$	$3/2^+ \Delta(1920)$	$5/2^+ \Delta(1905)$	$7/2^{+} \Delta(1950)$
2	$\mathbf{S}$	$2^{+}$	1/2	-	-	-	-
2	$\mathbf{S}$	$0_{+}$	3/2	-	$3/2^+ \Delta(1600)$	-	-
2	$\mathbf{S}$	$0_{+}$	1/2	-	-	-	-
1	Μ	1-	3/2	-	-	-	-
1	M	$1^{-}$	1/2	$1/2^- \Delta(1620)$	$3/2^- \Delta(1700)$	-	-
0	S	$0_{+}$	3/2	-	$3/2^+ \Delta(1232)$	-	
0	S	0+	1/2	-	-	-	

states and around 1900 MeV for  $\Delta$  states which is not reflected in models.

Furthermore, many more states are predicted than observed. This has been known for a long time as the 'missing resonance' problem [67]. Up to an excitation energy of 2.4 GeV, about 45 N states are predicted, but only 20 are established (four- or three-star; see Note on N and  $\Delta$  Resonances for the rating of the status of resonances) and 5 are tentative (two- or one-star). However, there is some recent progress. For the N=2 band, candidates have been identified for almost all predicted states with the exception of the  $(20,1_2^+)$ . Noteworthy is the recent addition of the new  $N(1880) 1/2^+$  state since the four states,  $N(1880) 1/2^+$ ,  $N(1900) 3/2^+$ ,  $N(2000) 5/2^+$ ,  $N(1990) 7/2^+$ , are considered to form a quartet of nucleon states with spin 3/2 and to be members of the  $(70,2_2^+)$  supermultiplet. The total number of states has perhaps not significantly changed but the number of states with four- or three-star rating has increased from 14 to 20 compared to the 2018 PDG particle listings. Most of this progress is due to the programs concentrating on the study of meson photoproduction reactions, while the most recent partial wave analysis of elastic pion scattering and charge exchange data by Arndt and collaborators [72] found no evidence for almost half of the states listed in this review (and included in Fig. 15.4). Such analyses are of course biased

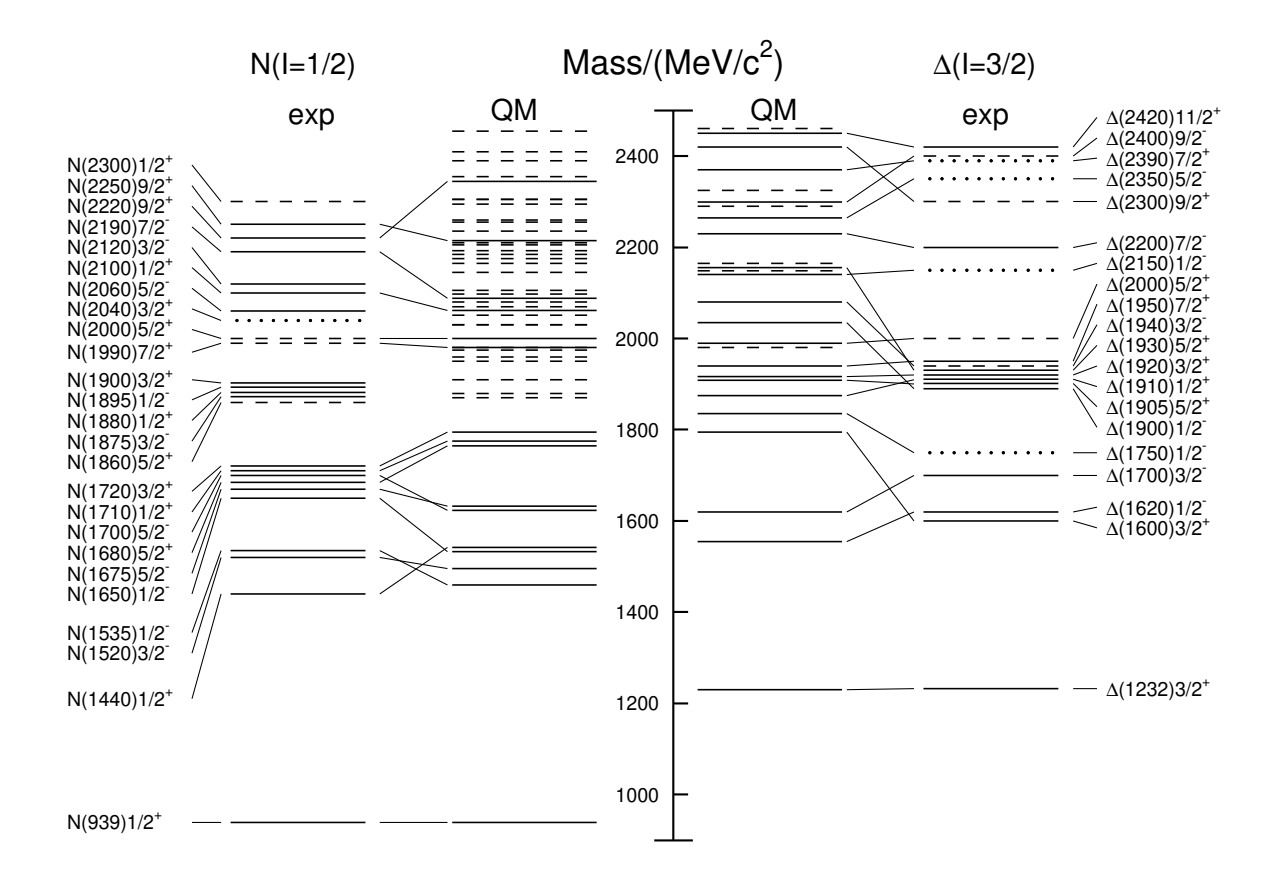


Figure 15.4: Excitation spectrum of the nucleon. Compared are the positions of the excited states identified in experiment, to those predicted by a relativized quark model calculation. Left hand side: isospin I=1/2 N-states, right hand side: isospin I=3/2  $\Delta$ -states. Experimental: (columns labeled 'exp'), three- and four-star states are indicated by full lines (two-star dashed lines, one-star dotted lines). At the very left and right of the figure, the spectroscopic notation of these states is given. Quark model [70,71]: (columns labeled 'QM'), all states for the N=1,2 bands, low-lying states for the N=3,4,5 bands. Full lines: at least tentative assignment to observed states, dashed lines: so far no observed counterparts. Many of the assignments between predicted and observed states are highly tentative.

against resonances which couple only weakly to the  $N\pi$  channel. Quark model predictions for the couplings to other hadronic channels and to photons are given in Ref. [70]. The large experimental effort ongoing at several electron accelerators to study the baryon resonance spectrum with real and virtual photon-induced meson production reactions includes the search for as-yet-unobserved states, as well as detailed studies of the properties of the low lying states (decay patterns, electromagnetic couplings, magnetic moments, etc.) (see Ref. [73] for reviews). There are two major new aspects of this program. The investigation of single and double polarization observables allows, via the study of interference terms, access to small partial waves that do not leave a footprint in unpolarized cross sections. An example for the impact of such data is given by a comparison of results from different multipole analyses of pion photoproduction [74]. It shows clearly that with the inclusion of polarization observables the reaction model results start to converge. This will in the near future much improve the database for excited baryons in the light quark sector.

The other aspect is the study of final states with meson pairs, in particular  $\pi\pi$  and  $\pi\eta$  pairs, which has made much progress during the last few years. This is important for higher lying states, which in the quark model may have both possible oscillations excited. Such states can be expected to decay in sequential processes de-exciting the two oscillations step-by-step so that they couple strongly to multiple-meson final states but not to single-meson production. Detailed analyses of such data are for example given in [75, 76] and had already significant impact on partial wave analyses.

The excitation spectrum of hyperons containing s-quarks is even less well explored. Many experimental results date back to before 2000, although parameters listed in the review are in many cases updated by more modern partial wave analyses. A recent review on the quark model interpretation of the  $\Lambda$  and  $\Sigma$  states is given in Ref. [77]. Significant progress on excited multistrange  $\Xi$  and  $\Omega$  states has been reported in recent years from the high-energy experiments, where these strange baryons are copiously produced in the decays of heavy baryons containing a charm or bottom quark, or in the decay of heavy-flavor mesons. A new  $\Omega^-$  state was reported in the  $\Xi K$  mass spectrum with high significance from the Belle experiment [78]. This  $\Omega(2012)^-$  resonance is fairly narrow and, therefore, has a likely  $J^P = \frac{3}{2}^-$  classification since the decay into  $\Xi K$  would proceed via D-wave. A state with  $J^P = \frac{1}{2}^-$  would decay via S-wave and thus be wider. The latest addition to the  $\Omega$  family,  $\Omega(2109)$ , was announced by the BES III Collaboration based on the reaction  $e^+e^- \to \Omega(2109)^-\bar{\Omega}^+$  [79]. It is interesting to note that the first radial excitation of the  $\Omega$  ground state is expected close to 2100 MeV.

In the doubly-strange sector, Belle reported on the most significant evidence so far for the  $\Xi(1620)$  in the  $\Xi\pi$  mass spectrum [80], which has warranted a recent upgrade of this resonance from one star to two stars. Most recently, the LHCb Collaboration has reported on the first observation of  $\Xi(1690)$  and  $\Xi(1820)$  in the decay of  $\Xi_b^-$  into  $J/\psi \Lambda K^-$  [81]. Masses and widths have been determined with improved precision in an amplitude analysis of the  $K^-\Lambda$  mass distribution. Evidence for these two states has also been reported by several other collaborations.

A recent review of strange  $\Xi$  and  $\Omega$  baryons is given in Ref. [82]. In the near future, significant progress on hyperon spectroscopy is expected from JLab using the  $K_L$  facility in conjunction with the GlueX exprimental setup, J-PARC using the  $K^-$  beam at the extended hadron facility, and the PANDA experiment at FAIR [83,84].

In quark models, the number of excited states is determined by the effective degrees of freedom. while their ordering and decay properties are related to the residual quark - quark interaction. An overview of quark models for baryons is given in [85], recent discussions of baryon spectroscopy are given in [65, 86]. The effective degrees of freedom in the standard nonrelativistic quark model are three equivalent valence quarks with one-gluon exchange-motivated, flavor-independent colormagnetic interactions. The QCD aspect of gluon-gluon interactions is emphasized by the hypercentral quark model [87,88], which includes in a natural way three-body forces between the quarks. A different class of models uses interactions which give rise to a quark - diquark clustering of the baryons: for a review see [89]. If there is a tightly bound diquark, only two degrees of freedom are available at low energies, and thus fewer states are predicted. Furthermore, selection rules in the decay pattern may arise from the quantum numbers of the diquark. However, we note that the recent identification of new  $N^*$  resonances seriously questions the older static diquark-quark model since these resonances are likely members of the  $(70,2_2^+)$ , which requires both oscillators in the baryon to be excited. More states are predicted by collective models of the baryon like the algebraic approach in [90]. In this approach, the quantum numbers of the valence quarks are distributed over a Y-shaped string-like configuration, and additional states arise e.g., from vibrations of the strings. More states are also predicted in the framework of flux-tube models, see [91], which are motivated by lattice QCD. In addition to the quark degrees of freedom, flux-tubes responsible for the confinement of the quarks are considered as degrees of freedom. These models include hybrid baryons containing explicit excitations of the gluon fields. However, since all half integral  $J^P$  quantum numbers are possible for ordinary baryons, such 'exotics' will be very hard to identify, and probably always mix with ordinary states. So far, the experimentally observed number of states is still far lower even than predicted by the quark–diquark models.

The influence of chiral symmetry on the excitation spectrum of the nucleon has been debated from a somewhat different perspective. Chiral symmetry, the fundamental symmetry of QCD, is strongly broken for the low lying states, resulting in large mass differences of parity partners like the  $J^P=1/2^+$   $N(938)1/2^+$  ground state and the  $J^P=1/2^ N(1535)1/2^-$  excitation. However, at higher excitation energies there is some evidence for parity doublets and even some very tentative suggestions for full chiral multiplets of  $N^*$  and  $\Delta$  resonances. An effective restoration of chiral symmetry at high excitation energies due to a decoupling from the quark condensate of the vacuum has been discussed (see [92] for recent reviews) as a possible cause. In this case, the mass generating mechanisms for low and high lying states would be essentially different. As a further consequence, the parity doublets would decouple from pions, so that experimental bias would be worse. However, parity doublets might also arise from the spin-orbital dynamics of the 3-quark system. Presently, the status of the data does not allow final conclusions.

The most recent developments on the theory side include progress in understanding the physics of baryons [93, 94] by using the Dyson-Schwinger equations of QCD and Bethe-Salpeter equations [95, 96]. In this approach, baryons are relativistic bound states of three quarks, and the treatment of their interactions arising from QCD is non-perturbative, incorporating aspects of confinement and dynamical symmetry breaking. Two paths to solving the three-body problem are taken: direct solution of the three-body Faddeev equation, and decomposition of baryons into quark-diquark systems, with all quark pairs able to constitute the diquark. Therefore, these descriptions are different from the older static diquark-quark pictures of the baryon. Moreover, the first unquenched lattice-QCD calculations for the excitation spectrum have been presented and are discussed in Sec. 15.8. The results are basically consistent with the level counting of  $SU(6) \otimes O(3)$  in the standard non-relativistic quark model and show no indication for quark-diquark structures or parity doubling. Consequently, there is as yet no indication from lattice that the mis-match between the excitation spectrum predicted by the standard quark model and experimental observations is due to inappropriate degrees of freedom in the quark model.

### 15.5.2 Charmed and bottom baryons

The naming scheme for baryons with c or b quarks follows that of the light baryons (see the Review on the "Naming Scheme for Hadrons"): the  $\Lambda$  is an isosinglet and the  $\Sigma$  an isotriplet with one heavy (s, c or b) quark. The  $\Xi$  is an isodoublet which contains two heavy quarks, and the  $\Omega$  an isosinglet with three heavy quarks. The number of c or b quarks is indicated by the subscripts c or b. Hyperons are baryons with at least one s quark. The antiparticle of the  $\Lambda_c^+$  (cud) is denoted  $\overline{\Lambda_c}$  (or simply  $\Lambda_c^-$ ), the antiparticle of the  $\Sigma_c^+$  is the  $\overline{\Sigma}_c^-$ .

For charmed baryons the addition of the c quark to the light quarks extends the flavor symmetry to  $\mathrm{SU}(4)_f$ . Due to the large mass of the c quark, this symmetry is much more strongly broken than the  $\mathrm{SU}(3)_f$  of the three light quarks. Nevertheless, the  $\mathrm{SU}(4)_f$  representation is still useful for bookkeeping purposes. With the additive charm quantum number C the baryons are classified in a 3-dimensional representation with the three coordinates ( I  $_z$ , Y , C ). Figure 15.5 shows the  $\mathrm{SU}(4)_f$  weight diagrams.

With four quarks the 64 possible configurations decompose into

$$\mathbf{4} \otimes \mathbf{4} \otimes \mathbf{4} = \bar{\mathbf{4}}_A \oplus \mathbf{20}_S \oplus \mathbf{20}_{MS} \oplus \mathbf{20}_{MA}, \tag{15.32}$$

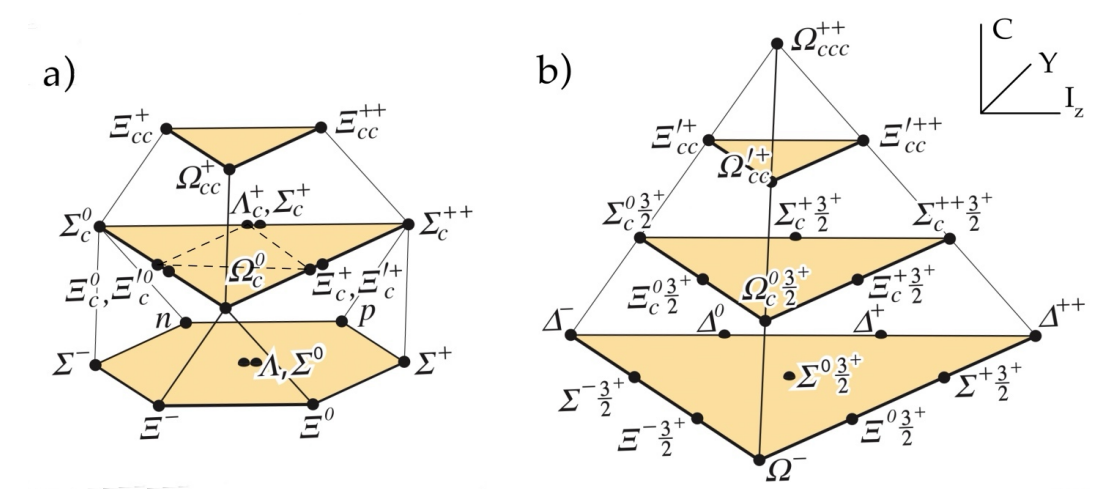


**Figure 15.5:** SU(4)<sub>f</sub> multiplets of ground state baryons made of u, d, s, and c quarks. (a) The spin  $\frac{1}{2}$  20-plet extends the charmless SU(3)<sub>f</sub> octet to C = 1, 2; (b) the spin  $\frac{3}{2}$  20-plet extends the SU(3)<sub>f</sub> decuplet to C = 1, 2, 3.

(for a review on SU(N) symmetries see e.g. [97]). The subscripts S and A refer to the symmetry and antisymmetry properties of the flavor wave functions. The flavor symmetric  $20_S$  multiplet, associated with spin- $\frac{3}{2}$  baryons, contains the charmless  $SU(3)_f$  decuplet at the bottom level. The  $20_{MS}$  and  $20_{MA}$  multiplets correspond to the mixed symmetric and mixed antisymmetric parts of the flavour wave functions of the spin- $\frac{1}{2}$  baryons, with the charmless octet baryons at the bottom level. There are two dsc and two usc spin- $\frac{1}{2}$  states, labeled  $\mathcal{Z}_c^0$ ,  $\mathcal{Z}_c^{\prime 0}$  and  $\mathcal{Z}_c^+$ ,  $\mathcal{Z}_c^{\prime +}$ . This is because one of the qq pairs can have spin 1 (symmetric) or spin 0 (antisymmetric), giving both the total spin  $j=\frac{1}{2}$  with the third quark (see also Fig. 15.6 below).

For  $\overline{C} = 1$  baryons the flavor decomposition of the diquark, made of u, d, or s quarks, is

$$\mathbf{3} \otimes \mathbf{3} = \bar{\mathbf{3}}_A \oplus \mathbf{6}_S. \tag{15.33}$$

For ground-state baryons, the overall antisymmetry of baryon wave function (including color) requires the light diquark to be symmetric under the exchange of spin and flavor, hence both symmetric or both antisymmetric, that is spin 1 for the  $\mathbf{6}_S$  and spin 0 for the  $\bar{\mathbf{3}}_A$ . The  $\bar{\mathbf{3}}$  then combines with the c quark to form the  $J^P = 1/2^+$  states, while the  $\mathbf{6}$  combines to form  $J^P = 1/2^+$  or  $J^P = 3/2^+$ . The weight diagrams of the  $\bar{\mathbf{3}}$  and  $\mathbf{6}$  ground-state representations are shown in Fig. 15.6. Within each multiplet the C = 1 baryons obey isospin and  $SU(3)_f$  mass relations at the expected orders.

The antisymmetric quadruplet in (15.32) does not exist in the ground state but is realized for the first orbital excitations (L=1). Figure 15.7 shows the weight diagram with the experimentally observed states. In the quark model the quadruplet consists of four baryon excitations with  $J^P=\frac{1}{2}$  and four excitations with  $\frac{3}{2}$ . The charmed ones are the partners of the  $\Lambda(1405)$  and  $\Lambda(1520)$  singlets of SU(3)<sub>f</sub>.

For a detailed review on charmed baryons see Ref. [82]. Quark model predictions for baryons with two heavy quarks are given in Ref. [98] and lattice results for doubly and triply charmed states are discussed in Sec. 15.8 of this *Review*.

The C=1 ground state baryons have all been observed. Due to their relatively narrow widths the states are much easier to isolate than the light quark baryon resonances which require intricate partial wave analyses. The production cross sections are small, but the recent measurements at the  $e^+e^-$  B-factories, at the  $p\bar{p}$  Tevatron collider, and at LHCb have boosted the field. The spin and

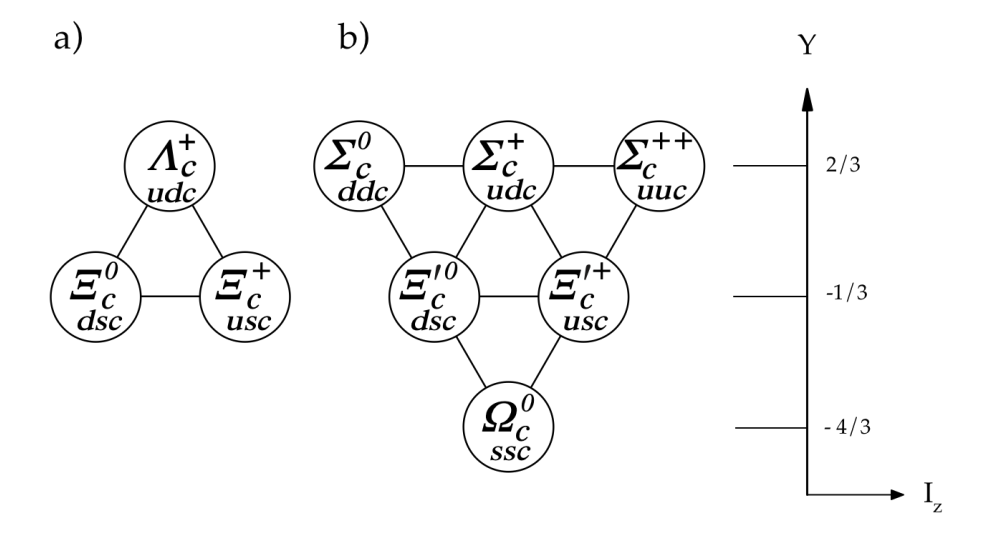


**Figure 15.6:** The SU(3)<sub>f</sub>  $\bar{\bf 3}$  (a) and  $\bf 6$  (b) ground state  $J^P=1/2^+$  representations. The structure of the  $\bf 6$  ground state with  $J^P=3/2^+$  is identical to the one in (b).

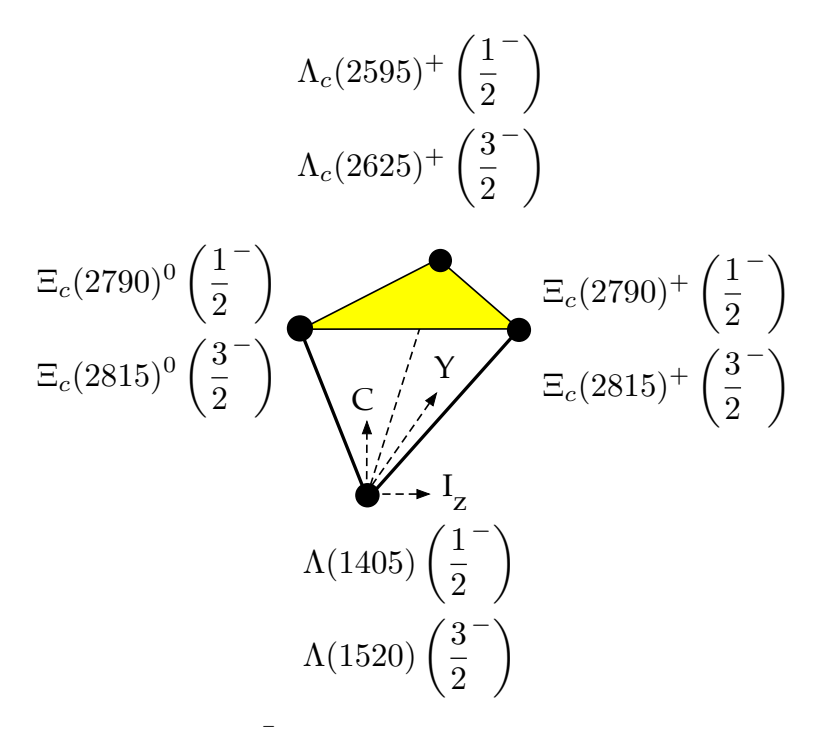


Figure 15.7: Weight diagram of the  $\bar{\bf 4}$  SU(4)<sub>f</sub> multiplet with the experimentally observed negative parity baryons.

parity of most charmed and bottom baryons has not been measured, they are from quark model predictions. The spin  $\frac{1}{2}$  of the  $\Lambda_c^+$  has been established by BES3 [99].

The LHCb collaboration has published evidence for seven new narrow  $\Omega_c^0$  states (css) [100,101] in proton-proton collisions. Four of these states have been confirmed by the Belle experiment in  $e^+e^-$  collisions [102]. Their quantum numbers are still unknown, but they could correspond to the L=1 ssc orbital excitations. Constituent quark models, lattice QCD, quark-diquark models,

molecular models, and pentaquark states, have been discussed to describe their structure (see e.g. [103] for references). In the meantime, also four  $\Omega_b^-$  states of the bss type have been reported from LHCb [103]. They lie in a narrow range between 6316 - 6350 MeV, but since their intrinsic widths are on the order of just a few MeV, they are well separated in the invariant mass spectra. Spectroscopy and theory in this field is rapidly evolving.

LHCb has observed a doubly charmed  $\Xi_{cc}^{++}$  (ccu) baryon decaying to  $\Lambda_c^+ K^- \pi^+ \pi^+$  [104],  $\Xi_c^+ \pi^+$  [105] and  $\Xi_c'^+ \pi^+$  [106]. The quantum numbers of this state are not known yet. Doubly charmed baryons have a very different structure from light baryons, more resembling heavy 'double-star' systems with attached light 'planets', which opens a new window for QCD properties. The first candidate for a doubly charmed baryon  $\Xi_{cc}^+$  (ccd) had been reported earlier by the SELEX experiment [107,108], but searches by other experiments have not confirmed it so far (see e.g. [109] and Refs. therein) and it is therefore not included in the Summary Table. The SELEX and LHCb masses lie in the predicted 3500 – 3700 MeV mass range (see e.g. [98]), but the LHCb  $\Xi_{cc}^{++}$  state lies about 100 MeV above the SELEX one, with a mass splitting far too large for ucc and dcc isospin partners. However, it has also been discussed that due to the different production mechanisms this is not necessarily a contradiction [110].

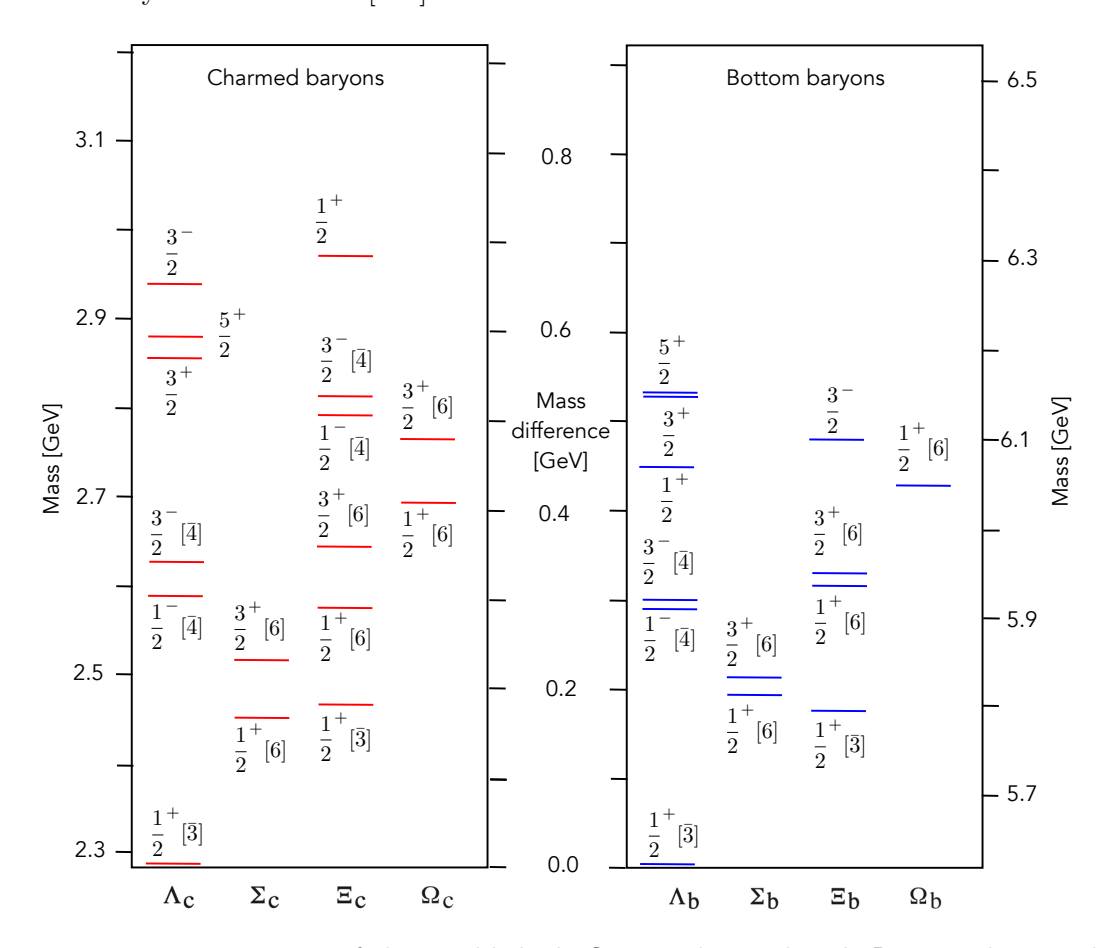


Figure 15.8: Mass spectrum of the established C = 1 charmed and B = -1 bottom baryons with known  $J^P$ , or assumed from the quark model. The flavor symmetry assignments (see 15.32) and (15.33) are given by the square brackets. According to their isospins the  $\Sigma_{c,b}$  ( $\Xi_{c,b}$ ) consist of three (two) charged or neutral states that are nearly degenerate.

Figure 15.8 shows the spectrum of the established singly-charmed baryons with known or as-

sumed quantum numbers from the quark model. The parity of the  $\Lambda_c^+$  is that of the c quark, defined as positive. Spin and parity have not been determined experimentally for most of the states. They follow the ordering and expectation from the quark model. Candidates for L=2 orbital excitations of the  $\Lambda_c$  (with  $J^P=\frac{3}{2}^+$  and  $J^P=\frac{5}{2}^+$ ) have already been observed, as well as a  $\frac{3}{2}^-$  state at 2940 MeV, possibly a radial L=1 excitation [111].

The same SU(4)<sub>f</sub> multiplets can be constructed for the bottom baryons by replacing the c quark by a b quark. Fig.15.8 shows the bottom baryons with known or assumed quantum numbers from the quark model. The quadruplet  $\bar{4}$  contains the two negative parity candidates  $\Lambda_b(5912)^0$  and  $\Lambda_b(5920)^0$ . It appears that the confining potential is only weakly flavour dependent. For example, the mass difference between the  $\Xi_b$  and the  $\Lambda_b$  is roughly the same as that between the  $\Xi_c$  and the  $\Lambda_c$ , the mass splitting between the spin- $\frac{1}{2}$   $\Omega_b$  and the  $\Lambda_b$  close to that between the spin- $\frac{1}{2}$   $\Omega_c$  and the  $\Lambda_c$ . The spin- $\frac{3}{2}$  states are also heavier than the spin- $\frac{1}{2}$  ones, in agreement with expectations from the spin-spin force. There are three  $\Xi_b$  excitations around 6100 MeV from LHCb and CMS [112,113]. Best established is the  $\Xi_b(6100)^-$ , an L=1 state with  $J^P=\frac{3}{2}$  according to the quark model.

The bottom hadrons can also be embedded in a larger  $SU(5)_f$  group that accounts for all baryons constructed from the five quark flavors. (The existence of baryons with t-quarks is very unlikely due to the short lifetime of the t-quark.) One predicts the decomposition

$$\mathbf{5} \otimes \mathbf{5} \otimes \mathbf{5} = \overline{\mathbf{10}}_{A} \oplus \mathbf{40}_{MS} \oplus \mathbf{40}_{MA} \oplus \mathbf{35}_{S}. \tag{15.34}$$

The decuplet is not realized in the ground state. The two 40-plets have mixed symmetry ( $\frac{1}{2}$ -spin) and the 35-plet is symmetric ( $\frac{3}{2}$ -spin). The SU(4)<sub>f</sub> spin- $\frac{1}{2}$  multiplet in Fig. 15.5 contains 20 spin- $\frac{1}{2}$  baryons and the corresponding one with bottom quarks an additional 12, giving together 32 states. Similarly there are 30 spin- $\frac{3}{2}$  baryons. One expects 75 ground state mesons from (15.34). Thus 13 ground state baryons containing both b and c quarks are predicted (8 spin- $\frac{1}{2}$  [ $4\Omega + 4\Xi$ ] and 5 spin- $\frac{3}{2}$  [ $3\Omega + 2\Xi$ ]).

### 15.6 Magnetic moments

The magnetic dipole moment of a baryon is conventionally written relative to the mass of the proton:

$$\vec{\mu}_B = q_B \mu_N \vec{s},\tag{15.35}$$

where  $\mu_N = \frac{e}{2m_p}$  is the nuclear magneton (in natural units). The factor  $g_B$  is calculated by adding the quark contributions. The magnetic moment of quark i with charge  $q_i e$  and constituent mass  $m_i$  is  $\vec{\mu}_i = 2(\frac{q_i e}{2m_i})\vec{s}$ , hence for the three light quarks,

$$\mu_u = \frac{2}{3}\kappa_u, \quad \mu_d = -\frac{1}{3}\kappa_d, \quad \mu_s = -\frac{1}{3}\kappa_s, \text{ with } \kappa_i \equiv \frac{e}{2m_i}.$$
 (15.36)

The magnetic dipole moment of a baryon is then given by

$$\mu_B = \sum_{i=1}^{3} \langle B \uparrow | \mu_i \sigma_{zi} | B \uparrow \rangle, \tag{15.37}$$

where  $|B\uparrow\rangle$  is the wavefunction for a baryon with its spin along the z-axis and  $\vec{\sigma}=2\vec{s}$ . Since the quark model uses the totally symmetric SU(6) wavefunctions (flavor SU(3) × spin SU(2)) one predicts for the proton:

$$\mu_p = \frac{4}{3}\mu_u - \frac{1}{3}\mu_d = \frac{e}{2m} \equiv \kappa,$$
(15.38)

assuming  $m_u = m_d \simeq m$  (for the detailed derivation see e.g. Ref. [6]). For the magnetic moment of the neutron one obtains likewise

$$\mu_n = -\frac{1}{3}\mu_u + \frac{4}{3}\mu_d = -\frac{2}{3}\kappa,\tag{15.39}$$

which leads to the simple prediction  $\mu_n/\mu_p = g_n/g_p = -2/3$ .

The famous Frisch and Stern experiment showed for the first time that  $g_p \sim 5.58 \gg 2$ . Modern measurements are performed in electromagnetic traps, see the *Listings*, while the magnetic moment of the neutron is measured with cold neutron beams. The experimental ratio  $\mu_n/\mu_p = -0.6849793 \pm 0.0000003$  is impressively close to the prediction of the quark model (note that using instead the antisymmetric SU(6) wavefunctions would lead to  $\mu_n/\mu_p = -2$  [6]). The constituent mass m of the u and d quarks can be estimated from (15.35) and (15.38):  $m = 2m_p/g_p \simeq 336$  MeV.

The magnetic moment of the  $\Lambda$  is easy to predict: the diquark ud has isospin i=0, since i(s)=0 and  $i(\Lambda)=0$ , and is therefore an antisymmetric isospin state. The symmetric quark model then also requires the spin to be zero, so that the magnetic moment of the  $\Lambda$  stems from the s quark:

$$\mu_{\Lambda} = \mu_s = -\frac{1}{3}\kappa_s. \tag{15.40}$$

The magnetic moment of the  $\Lambda$  is obtained from the Larmor precession frequency of the polarization vector in an homogeneous magnetic field. The latter is derived from the asymmetric distribution of the proton in  $\Lambda \to \pi^- p$  [114]. The experimental result (Table 15.8) leads to the s quark constituent mass  $m_s = -m\mu_p/3\mu_{\Lambda} = 509$  MeV.

**Table 15.8:** Quark model predictions and measured magnetic dipole moments of the ground state baryons in units of  $\mu_N$ ;  $\kappa \equiv \frac{e}{2m} = 2.793 \ \mu_N$  and  $\kappa_s \equiv \frac{e}{2m_s} = -3\mu_{\Lambda} = 1.84 \ \mu_N$ .  $^{\dagger}\Sigma^0 \to \Lambda$  transition magnetic moment; ‡ see also Ref. [115].

Baryon	Quark 1	noc	lel	Experin	ient	al value
$\overline{p}$	κ		input	2.793		
n	$-\frac{2}{3}\kappa$	=	-1.86	-1.913		
$\Lambda$	$-\frac{1}{3}\kappa_s$		input	-0.6138	$\pm$	0.0047
$\Sigma^+$	$\frac{8}{9}\kappa + \frac{1}{9}\kappa_s$	=	2.68	2.458	$\pm$	0.010
$\Sigma^0$	$\frac{2}{9}\kappa + \frac{1}{9}\kappa_s$	=	0.82			
$\Sigma^{0\dagger}$	$-\frac{1}{\sqrt{3}}\kappa$	=	-1.61	-1.61	$\pm$	0.08
$\Sigma^-$	$-\frac{4}{9}\kappa + \frac{1}{9}\kappa_s$	=	-1.04	-1.160	$\pm$	0.025
$\Xi^0$	$-\frac{2}{9}\kappa - \frac{4}{9}\kappa_s$	=	-1.44	-1.250	$\pm$	0.014
$\varXi^-$	$\frac{1}{9}\kappa - \frac{4}{9}\kappa_s$	=	-0.51	-0.6507	$\pm$	0.0025
$\Omega^-$	$-\kappa_s$	=	-1.84	-2.024	$\pm$	0.056
$\Delta^{++}$	$2\kappa$	=	5.58	4.52	$\pm$	$0.67 \ \ddagger$
$\Delta^+$	$\kappa$	=	2.79	2.3	-	4.5

The magnetic moments of the other baryons (Table 15.8) are predicted from  $\kappa$  and  $\kappa_s$ . The magnetic moment of the  $\Sigma^+$  is obtained by replacing the d quark in (15.38) by an s quark, and for the  $\Sigma^-$  the u quark by an s quark in (15.39). The magnetic moment of the  $\Sigma^+$  has also been measured with the precession method using its decay into  $p\pi^0$  [116], that of the  $\Sigma^- \to n\pi^-$ 

likewise, or by detecting the X-rays emitted by cascading  $\Sigma^-$  captured in the Coulomb shells of target atoms. The magnetic moment is then derived from the fine-structure splitting [117].

The magnetic moments of the  $\Xi^0$ ,  $\Xi^-$  and  $\Omega^-$  are obtained from the polarization of the  $\Lambda$  in the decays  $\Lambda\pi^0$ ,  $\Lambda\pi^-$  and  $\Lambda K^-$ , respectively. The SU(6) wavefunction of the (spin 3/2)  $\Omega^-$  is the product of the two symmetric SU(3) flavor and SU(2) spin wavefunctions. Summing over the three s quarks one gets

$$\mu_{\Omega^{-}} = \sum_{i=1}^{3} \langle \Omega^{-} \uparrow | \mu_{i} \sigma_{zi} | \Omega^{-} \uparrow \rangle = 3\mu_{s} = 3\mu_{\Lambda}. \tag{15.41}$$

The magnetic moment of the  $\Omega^-$  is hard to measure, because the  $\Omega^-$  is unpolarized at high energies, in contrast to the other hyperons. Polarized  $\Omega^-$  hyperons have been obtained from polarized  $\Lambda$  and  $\Xi^0$  impinging on a nuclear target [118].

In quark models with full isospin symmetry the magnetic moments of the  $\Delta$ -resonances are simply related to the magnetic moment of the proton by  $\mu_{\Delta} = Q_{\Delta} \cdot \mu_{N}$ ,  $(Q_{\Delta} = \text{charge})$  i.e. the moment of the  $\Delta^{+}$  should equal the proton moment and the moment of the  $\Delta^{++}$  should be twice as large (sum of the three u-quarks). Magnetic moments of the decuplet baryons (with the exception of the  $\Omega^{-}$ ) are very difficult to measure because their lifetimes are so short that spin precession techniques cannot be used. For the  $\Delta$  one can profit from an electromagnetic spin-reorientation transition inside the large width of the state. This leads to the emission of a magnetic dipole photon in reactions like  $\pi^{+}p \to \pi^{+}p\gamma$  or  $\gamma p \to \pi^{0}p\gamma'$  which is related to the magnetic moment of the resonance. The first reaction has been used to study the magnetic moment of the  $\Delta^{++}$  by measuring the left-right asymmetry with polarized protons [119]. The second one was used for the  $\Delta^{+}$  state [120, 121]. Taking all experimental and systematic uncertainties into account the result spans the range from (2.3 - 4.5) $\mu_{N}$ , covering the quark model prediction of  $\approx 2.8\mu_{N}$ , but is not very precise.

Table 15.8 lists the current experimental values for the magnetic moments of the ground state baryons, together with the predictions from the quark model. There are significant discrepancies, but given its crudeness, the quark model performs surprisingly well.

#### 15.7 Dynamics

Quantum chromodynamics (QCD) is well-established as the theory for the strong interactions. As such, one of the goals of QCD is to predict the spectrum of strongly-interacting particles. To date, the only first-principles calculations of spectroscopy from QCD use lattice methods. These are the subject of Sec. 15.8. These calculations are difficult and unwieldy, and many interesting questions do not have a good lattice-based method of solution. Therefore, it is natural to build models, whose ingredients are abstracted from QCD, or from the low-energy limit of QCD (such as chiral Lagrangians) or from the data itself.

Phenomenological models for light quark systems typically include

- 1. A confining interaction, which is generally spin-independent (e.g., harmonic oscillator or linear confinement);
- 2. A strange quark mass somewhat larger than the up and down quark masses, in order to split the SU(3) multiplets;
- 3. Different types of spin-dependent interactions:
  - a) commonly used is a color-magnetic flavor-independent interaction modeled after the effects of gluon exchange in QCD (see e.g., Ref. [122]). For example, in the S-wave states, there is

a spin-spin hyperfine interaction of the form

$$H_{HF} = -\alpha_S M \sum_{i>j} (\vec{\sigma}\lambda_a)_i (\vec{\sigma}\lambda_a)_j, \qquad (15.42)$$

where M is a constant with units of energy,  $\lambda_a$  ( $a=1,\dots,8$ ,) is the set of SU(3) unitary spin matrices, defined in the review "SU(3) Isoscalar Factors and Representation Matrices," and the sum runs over constituent quarks or antiquarks. Spin-orbit interactions, although allowed, seem to be small in general, but a tensor term is responsible for the mixing of states with the same  $J^P$  but different L, S combinations.

b) other approaches include flavor-dependent short-range quark forces from instanton effects (see e.g., [123,124]). This interaction acts only on scalar, isoscalar pairs of quarks in a relative S-wave state:

$$\langle q^2; S, L, T | W | q^2; S, L, T \rangle = -4g \delta_{S,0} \delta_{L,0} \delta_{L,0} \mathcal{W}$$
 (15.43)

where W is the radial matrix element of the contact interaction.

c) a rather different and somewhat controversial approach is based on flavor-dependent spinspin forces arising from one-boson exchange. The interaction term is of the form:

$$H_{HF} \propto \sum_{i < j} V(\vec{r}_{ij}) \lambda_i^F \cdot \lambda_j^F \vec{\sigma}_i \cdot \vec{\sigma}_j$$
 (15.44)

where the  $\lambda_i^F$  are in flavor space (see e.g., [125]).

4. In the case of spin-spin interactions, a flavor-symmetric interaction for mixing  $q\bar{q}$  configurations of different flavors  $(e.g., u\bar{u} \leftrightarrow d\bar{d} \leftrightarrow s\bar{s})$ , in isoscalar channels, so as to reproduce e.g., the  $\eta$  -  $\eta'$  and  $\omega$  -  $\phi$  mesons.

Systems with heavy quarks have their own approaches. Besides potential models to deal with  $Q\bar{Q}$  spectroscopy (which are similar to what we have just described for light quarks) there are a variety of effective field theories built on QCD. Nonrelativistic QCD or NRQCD is a nonrelativistic reduction of the QCD Lagrangian, written as an expansion in powers of the heavy quarks' velocities. Its expressions are often used in lattice calculations. Terms in the Lagrangian have obvious quark model analogs, but are derived directly from QCD. For example, the heavy quark potential is a derived quantity, extracted from simulations.

There are also many versions of heavy quark effective theory (HQET), an expansion in the inverse mass of the heavy constituent. The physics input is one of decoupling of scales: the interactions of the heavy quarks take place at short distance while the light degrees of freedom involve long distance dynamics, so to some degree they decouple. The form of terms in the expansion is fixed (often by symmetry) but the coefficients are not. These approaches allow one to interpolate from the charm sector to the bottom one, or from masses of mesons to baryons. For example, a Hamiltonian for one or more heavy quarks bound to light degrees of freedom could be written as

$$H_l^Q = m_Q + e_l + \frac{\kappa_l}{2m_Q} + \frac{s_l}{2m_Q} \vec{S} \cdot \vec{j}_l + \dots$$
 (15.45)

where  $m_Q$  is the mass of the heavy quark (or heavy quarks where the heavy quarks are treated as a single dynamical object) and  $\vec{S}$  is the angular momentum carried by the heavy degrees of freedom.  $e_l$ ,  $\kappa_l$  and  $\vec{j}_l$  involve the light degrees of freedom. We will see an example of the use of this formula in the next section.

# 15.8 Lattice Calculations of Hadronic Spectroscopy

Lattice calculations are a major source of information about QCD masses and matrix elements. The necessary theoretical background is given in Sec. 17 of this *Review*. Here we confine ourselves to some general comments and illustrations of lattice calculations for spectroscopy.

It might seem a bit out of place to have a section about lattice calculations in a review of the quark model, since to many readers, the quark model is just a model while QCD could be thought of as a construct which is something deeper than a model. But this review is, despite its title, actually an introduction to the spectroscopy and related quantities of the strong interactions. From that perspective, a presentation of lattice results is entirely appropriate.

The input to lattice calculations is a discretized version of the QCD Lagrangian. Lattice calculations measure correlation functions via Monte Carlo simulation and physical observables are determined through fits of the lattice data to theoretical expectations. It is fair to say that all lattice calculations make extensive use of quark model ideas – for example, the operators used to create and annihilate hadrons are almost always based on the quark model.

There is only a sporadic literature connecting lattice results to the quark model (one recent example is [126]) but of course the qualitative understanding of lattice results depends as heavily on quark model ideas as does the qualitative understanding of experimental data.

In general, the cleanest lattice results come from computations of processes in which there is only one particle in the simulation volume. These quantities include masses of hadrons, simple decay constants, like pseudoscalar meson decay constants, and semileptonic form factors (such as the ones appropriate to  $B \to Dl\nu$ ,  $Kl\nu$ ,  $\pi l\nu$ ). The cleanest predictions for masses are for states which are far below any thresholds to open channels, since the effects of final state interactions are not yet under complete control on the lattice. As a simple corollary, the lightest state in a channel is easier to study than the heavier ones.

Good-quality modern lattice calculations will present multi-part error budgets with their predictions. Part of the uncertainty is statistical, from sample size. Typically, the quoted statistical uncertainty includes uncertainty from a fit: it is rare that a simulation computes one global quantity which is the desired observable. Simulations which include virtual quark-antiquark pairs (also known as "dynamical quarks" or "sea quarks") are often done at up and down quark mass values heavier than the experimental ones, and it is then necessary to extrapolate in these quark masses. Simulations can be carried out at the physical values of the heavier quarks' masses. They are always done at nonzero lattice spacing, and so it is necessary to extrapolate to zero lattice spacing. Some theoretical input is needed to do this. Much of the uncertainty in these extrapolations is systematic, from the choice of fitting function. Other systematics include the effect of finite simulation volume, the number of flavors of dynamical quarks actually simulated, and technical issues with how these dynamical quarks are included. The particular choice of a fiducial mass (to normalize other predictions) is not standardized; there are many possible choices, each with its own set of strengths and weaknesses, and determining it usually requires a second lattice simulation from that used to calculate the quantity under consideration.

A systematic error of major historical interest is the "quenched approximation," in which dynamical quarks are simply left out of the simulation. This was done because the addition of these virtual pairs presented an expensive computational problem. No generally-accepted methodology has ever allowed one to correct for quenching effects, short of redoing all calculations with dynamical quarks. (All light degrees of freedom must be included in any realistic simulation of a quantum field theory.) Advances in algorithms and computer hardware have rendered it obsolete.

With these brief remarks, we turn to examples. The field of lattice QCD simulations is vast, and so it is not possible to give a comprehensive review of them in a small space. The history of lattice QCD simulations is a story of thirty years of incremental improvements in physical understanding,

algorithm development, and ever faster computers, which have combined to bring the field to a present state where it is possible to carry out very high quality calculations. We present a few representative illustrations, to show the current state of the art.

### 15.8.1 Spectroscopy of low-lying states

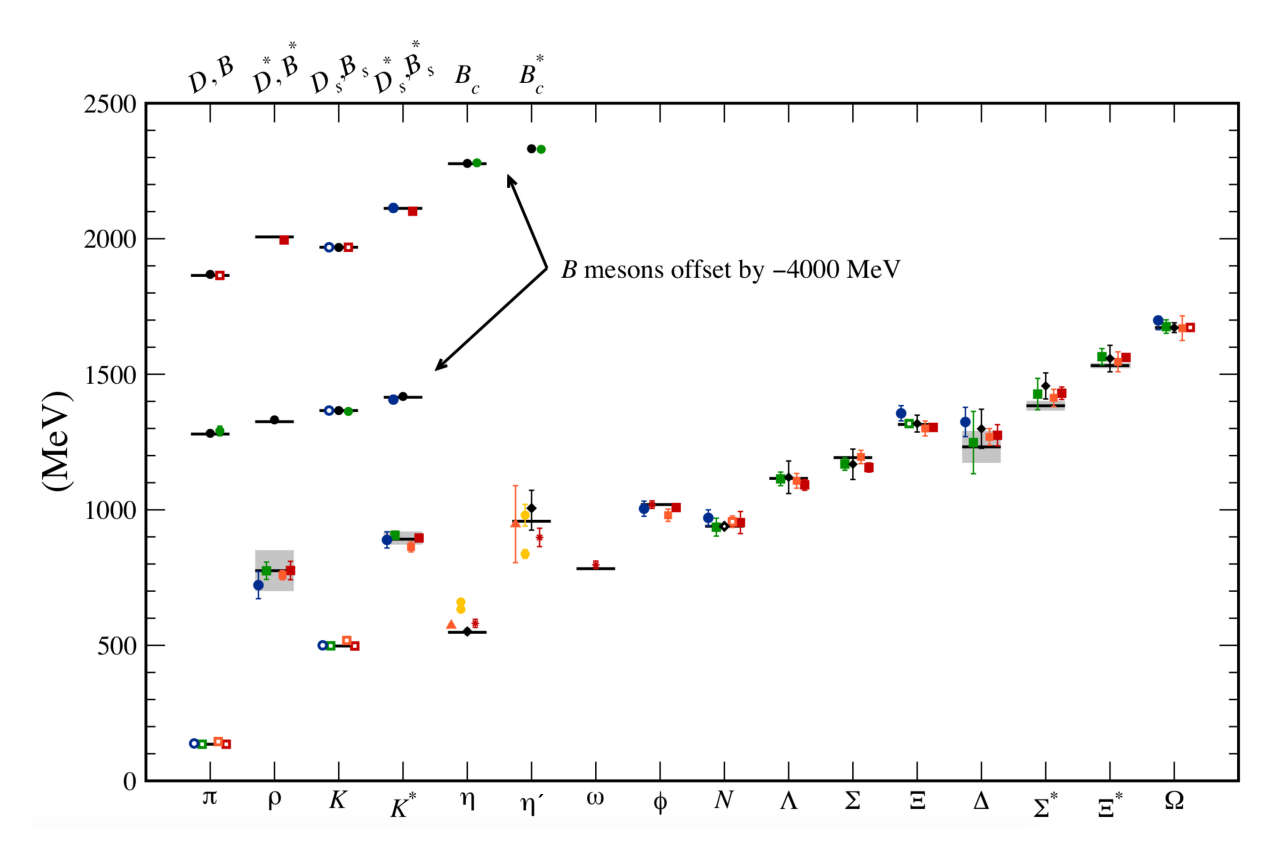


Figure 15.9: Hadron spectrum from lattice QCD. Comprehensive results for mesons and baryons are from MILC [127,128], PACS-CS [129], BMW [130], QCDSF [131], and ETM [132]. Results for  $\eta$  and  $\eta'$  are from RBC & UKQCD [21], Hadron Spectrum [133] (also the only  $\omega$  mass), UKQCD [134], and Michael, Ottnad, and Urbach [135]. Results for heavy-light hadrons from Fermilab-MILC [136], HPQCD [137,138], and Mohler and Woloshyn [139]. Circles, squares, diamonds, and triangles stand for staggered, Wilson, twisted-mass Wilson, and chiral sea quarks, respectively. Asterisks represent anisotropic lattices. Open symbols denote the masses used to fix parameters. Filled symbols (and asterisks) denote results. Red, orange, yellow, green, and blue stand for increasing numbers of ensembles (i.e., lattice spacing and sea quark mass) Black symbols stand for results with 2+1+1 flavors of sea quarks. Horizontal bars (gray boxes) denote experimentally measured masses (widths). b-flavored meson masses are offset by -4000 MeV.

One of the first goals of large scale lattice simulations was to compute masses of the lightest states in all of the "conventional"  $q\bar{q}$  and qqq channels. We illustrate results from many groups in Fig. 15.9, a comprehensive summary from 2012 provided by A. Kronfeld (private communication; see also [140]).

Mesons with a valence structure of identical quark - antiquark pairs such as the eta or eta-prime,  $|\eta\rangle \sim \alpha |\bar{u}u + \bar{d}d\rangle + \beta |\bar{s}s\rangle$ , present more of a challenge, because one must include the effects of "annihilation graphs" for the valence q and  $\bar{q}$ . Many groups, among them Refs. [21, 134, 141, 142], have reported calculations of the  $\eta$  and  $\eta'$  mesons. The most recent calculation is that of Ref. [142],

which finds masses of  $554.7 \pm 9.2$  and  $930 \pm 21$  MeV for the  $\eta$  and  $\eta'$ .

The spectroscopy of mesons containing heavy quarks is truly a high-precision endeavor. These simulations typically use NRQCD for  $Q\bar{Q}$  bound states. Figs. 15.10 and 15.11 show the low lying mass spectrum for charmonium and bottomonium states from several different groups [138,143–146]. Most, but not all, of the results are for the lightest state with a given value of quantum numbers. We return to this point below.

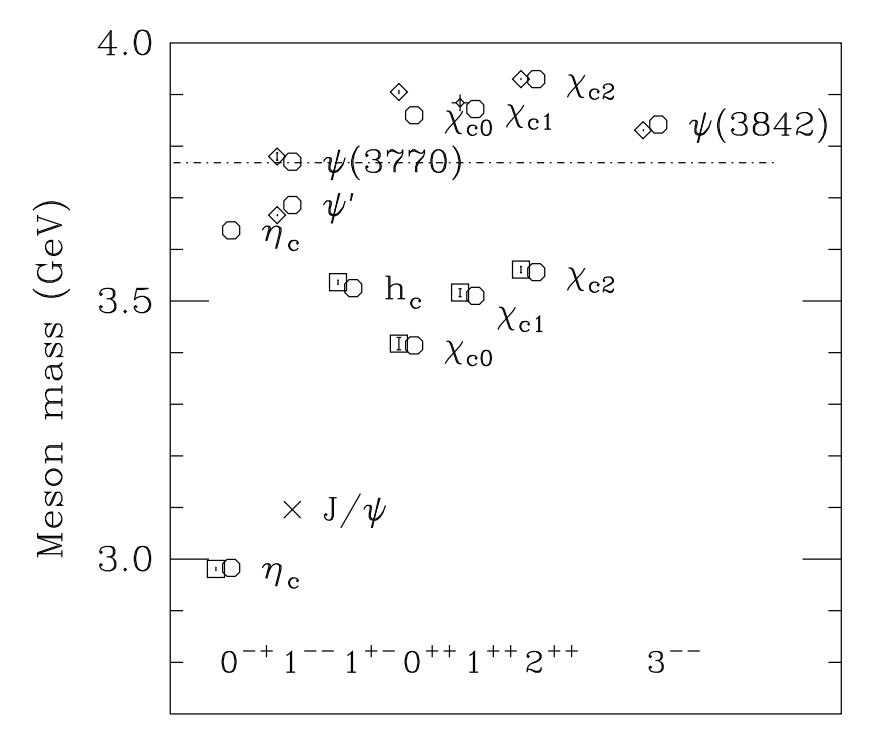


Figure 15.10: Selected spectroscopy of the  $\bar{c}c$  spectrum, compared to lattice data from Ref. [143] in squares, from Refs. [144, 145] in diamonds, and from Ref. [146] as a fancy diamond. Particles whose masses are used to fix lattice parameters by Ref. [143] are shown with crosses; octagons label experimental values. The upper  $\chi_{c1}$  state is also known as X(3872). The dotted line shows the threshold value for two charmed mesons.

Fig. 15.12 shows a compilation of lattice results for doubly and triply charmed baryons, provided by S. Meinel [154]. The position of the observed  $\Xi_{cc}^+$  [104] is also shown. Note that the lattice calculations for the mass of this state were predictions, not postdictions.

#### 15.8.2 Excited state spectroscopy

A close look at Fig. 15.9 reveals an issue: while many of the states shown in it are stable under the strong interactions, some of them (the vector mesons, the Delta) are not. They are resonances. And so are all the excited states of hadrons listed in the PDG be they "ordinary"," or "exotic." How do lattice calculations deal with such states? This is actually a complicated business, which is an active area of research.

There are two issues involving excited state spectroscopy, which are entangled in any lattice calculation:

- 1. There are many states with the same quantum numbers, all of which contribute to lattice observables
- 2. In finite volume, states do not decay, they only mix.

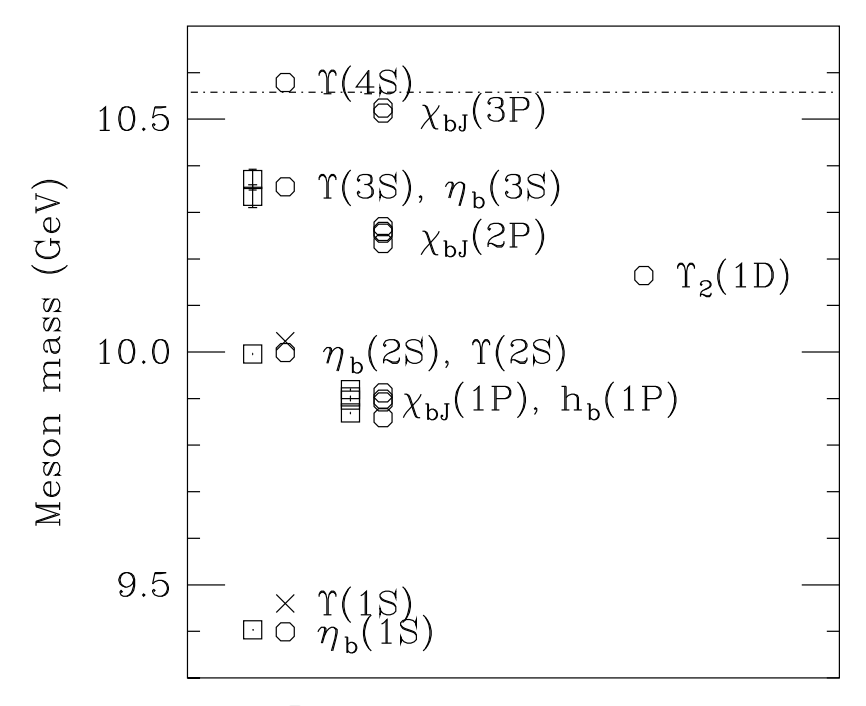


Figure 15.11: Spectroscopy of the  $\bar{b}b$  system, adapted from Ref. [138]. Particles whose masses are used to fix lattice parameters are shown with crosses; octagons label experimental values, and lattice results are shown as squares. The dotted line shows the threshold value for two bottom mesons.

To explain what is going on, we have to describe how a lattice calculation determines a mass. This is done by measuring an observable which involves the creation of a set of quark and gluon fields at some point on the lattice and their annihilation at other points on the lattice. To find the energies of zero momentum states, the operators are averaged over position and the observable is

$$C_{ij}(t) = \sum_{x} \langle O_i(x, t) O_j(0, 0) \rangle \propto \sum_{n} \langle 0 | O_i | n \rangle \langle n | O_j | 0 \rangle \exp(-E_n t).$$
 (15.46)

 $E_n$  is the energy of the *n*th hadronic state with the quantum numbers of the source or sink. The reader can see that by taking t large, the correlator is dominated by the contribution from the lightest state, decaying with t as  $\exp(-E_{min}t)$ . This is a positive thing if one is interested in the ground state, but the contribution of excited states is exponentially suppressed at large t. The size of a given state's contribution,  $\langle 0|O_i|n\rangle$ , can provide information about the content of the state.

As we move away from hadrons which can be created by the simplest quark model operators (appropriate to the lightest meson and baryon multiplets) we encounter a host of new problems: either no good interpolating fields, or too many possible interpolating fields, and many states with the same quantum numbers. Techniques for dealing with these interrelated problems vary from collaboration to collaboration, but all share common features: typically, correlation functions from many different interpolating fields are used, and the signal is extracted in what amounts to a variational calculation using the chosen operator basis. In addition to mass spectra, wave function information can be garnered from the form of the best variational wave function.

These calculations give towers of excited states, but the states are not resonances. Lattice calculations do not see decays directly because they are done in boxes of some finite size. Generally, the energies of the single particle states do not depend strongly on the box size. Multiple particle states, such as two particle states with equal and opposite momenta, are different, though. The

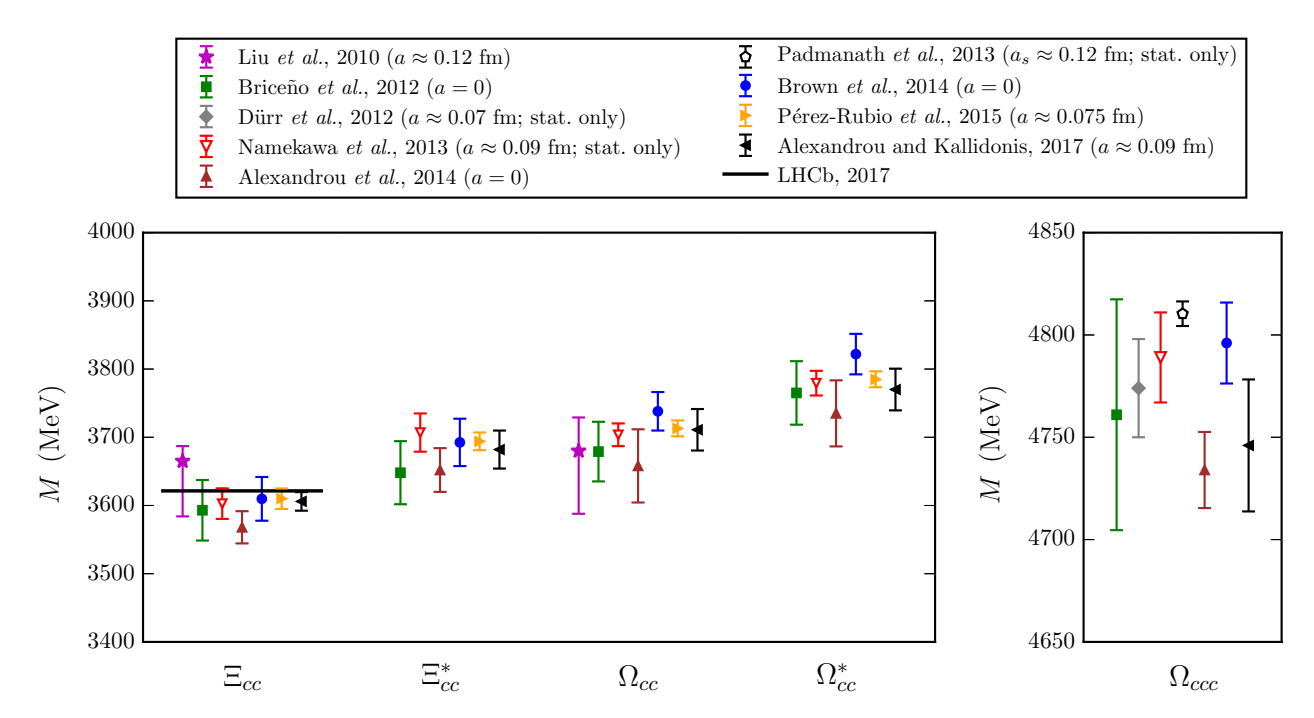


Figure 15.12: Comparison of lattice QCD results for the doubly and triply charmed baryon masses. Labels are Liu, et al., [147]; Briceno, et al., [148]; Namekawa, et al., [149]; Padmanath, et al., [150]; Alexandrou, et al., [132]; Brown, et al., [151]; Perez-Rubio et al., [152]; Alexandrou and Kallidonis 2017, [153]. Only calculations with dynamical light quarks are included; for the doubly charmed baryons, only calculations were performed at or extrapolated to the physical pion mass are shown. Results without estimates of systematic uncertainties are labeled "stat. only". The lattice spacing values used in the calculations are also given; a = 0 indicates that the results have been extrapolated to the continuum limit. In the plot of the doubly charmed baryons, the position of the experimentally observed  $\Xi_{cc}^+$  state [104] is shown with a horizontal line.

finite box size quantizes the allowed values of momentum and the spectrum of states, which would be a continuum in infinite volume, is just a discrete tower. As the box size is varied, some of these states can approach the energies of single particle states, and the nearby states will mix and split, participating in a quantum mechanical avoided level crossing. The mixing and splitting of single and multiparticle states is the finite volume data which is used to infer how states in the continuum interact.

As a simple example, two positive energy but interacting particles in a one dimensional box have a spatial wave function which looks like  $\cos(k|z|+\delta)$  where  $\delta$  is the phase shift due to their interaction. Periodic boundary conditions in a finite box of length L give a quantization condition to the allowed momentum of the state  $(kL+2\delta(E)=0 \mod 2\pi)$ , for example) which involves the phase shift. Simulations with many values of L and operators for states carrying many values of momentum can be combined into information about phase shifts, and then to statements about the location(s) of singularities in the complex energy plane.

The techniques for studying excited states of mesons and baryons, glueballs, and exotics are similar. They all use a large basis of trial states: the progression with time started with minimum quark content states, then added more complicated states (pairs of mesons or tetraquark states), then carried out simulations with multiple volumes with the goal of extracting resonance properties. The older single volume studies typically presented results for many quantum numbers, which give

a broad (though incomplete) view of the QCD spectrum.

An example of meson spectroscopy where this is done, by [53], is shown in Fig. 15.13. The quark masses are still heavier than their physical values, so the pion is at 392 MeV. The authors can assign a relative composition of nonstrange and strange quark content to their states, observing, for example, a nonstrange  $\omega$  and a strange  $\phi$ . Some states also have a substantial component of gluonic excitation. Note especially the three exotic channels  $J^{PC} = 1^{-+}$ ,  $0^{+-}$ , and  $2^{+-}$ , with states around 2 GeV. These calculations will become more realistic as the quark masses are carried lower and resonance effects are included.

The interesting physics questions of excited baryon spectroscopy to be addressed are precisely those enumerated in the last section. An example of a calculation involving only single particle states in a single volume, due to Ref. [155], is shown in Fig. 15.14. Notice that the pion is not yet at its physical value. The lightest positive parity state is the nucleon, and the Roper resonance has not yet appeared as a light state.

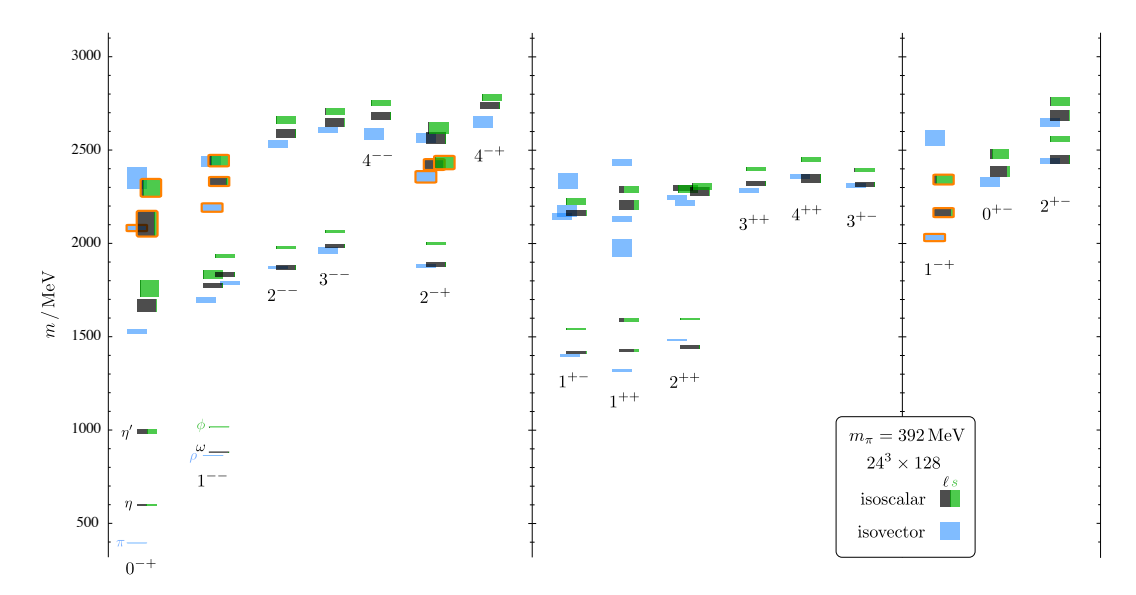
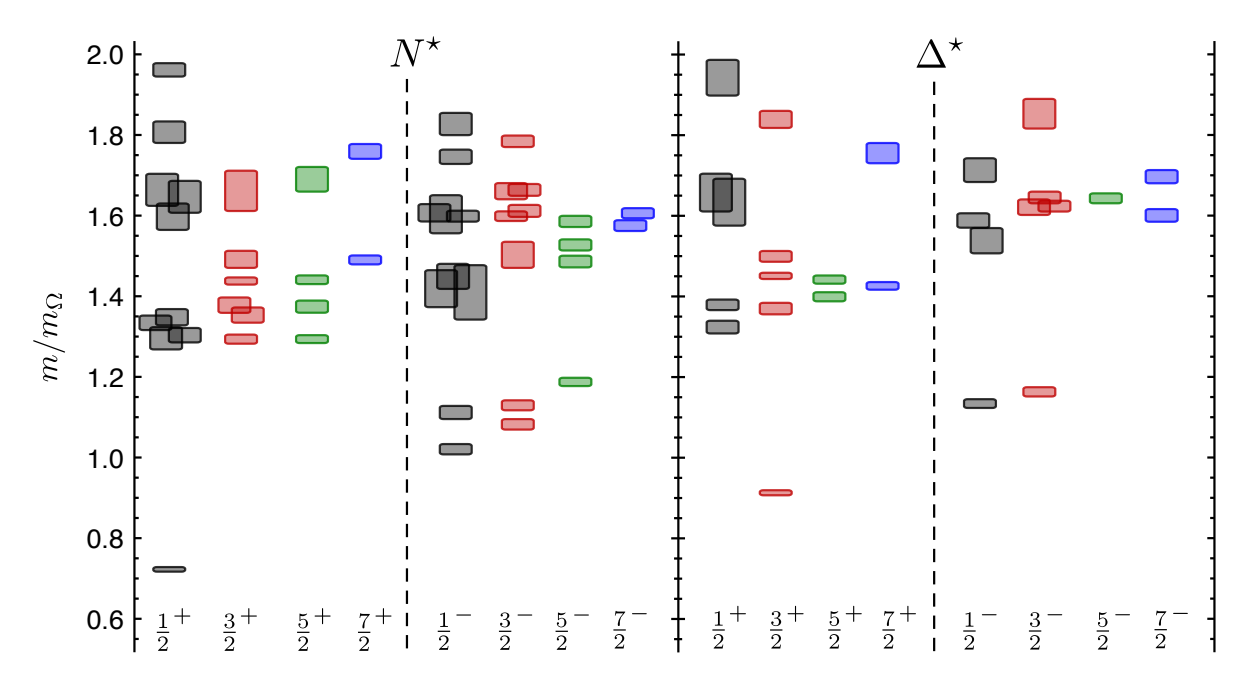


Figure 15.13: Isoscalar (green and black) and isovector (blue) spectrum from Ref. [53]. States are labeled  $J^{PC}$ . The quark mass is heavier than its physical value;  $m_{\pi}=392$  MeV. The vertical height of each box indicates the statistical uncertainty in the mass. Black and green indicate relative nonstrange and strange composition. Orange outlines show states with a large chromomagnetic component to their wave function, which the authors argue are hybrid states. Note the exotic states in the three rightmost columns.

Glueballs present similar issues. In Fig. 15.3 we showed a figure from [35] presenting a lattice prediction for the glueball mass spectrum in quenched approximation. A true QCD prediction of the glueball spectrum requires dynamical light quarks, some way to deal with the mixing of glue states and quark-antiquark (and beyond) states and (because glueball operators are intrinsically noisy) high statistics. Early studies which include the  $0^{++}$  channel are Refs. [156,157]. Fig. 15.15 shows results from [156], done with dynamical u, d and s quarks at two lattice spacings, 0.123 and 0.092 fm, with pion masses at 280 and 360 MeV respectively, along with comparisons to the quenched lattice calculation of [34] and to experimental isosinglet mesons. This study shows that the effects of quenching seem to be small at its relatively heavy pion masses. A recent review [158] concludes "no scalar state below 2 GeV can be considered to be predominantly a glueball state."

Calculations of resonance properties are more recent. Two body decays with a single open



**Figure 15.14:** Spin-identified spectrum of nucleons and deltas, from lattices where  $m_{\pi}=396$  MeV, in units of the calculated  $\Omega$  mass, from Ref. [155]. The colors just correspond to the different J assignments: grey for J=1/2, red for J=3/2, green for 5/2, blue for J=7/2.

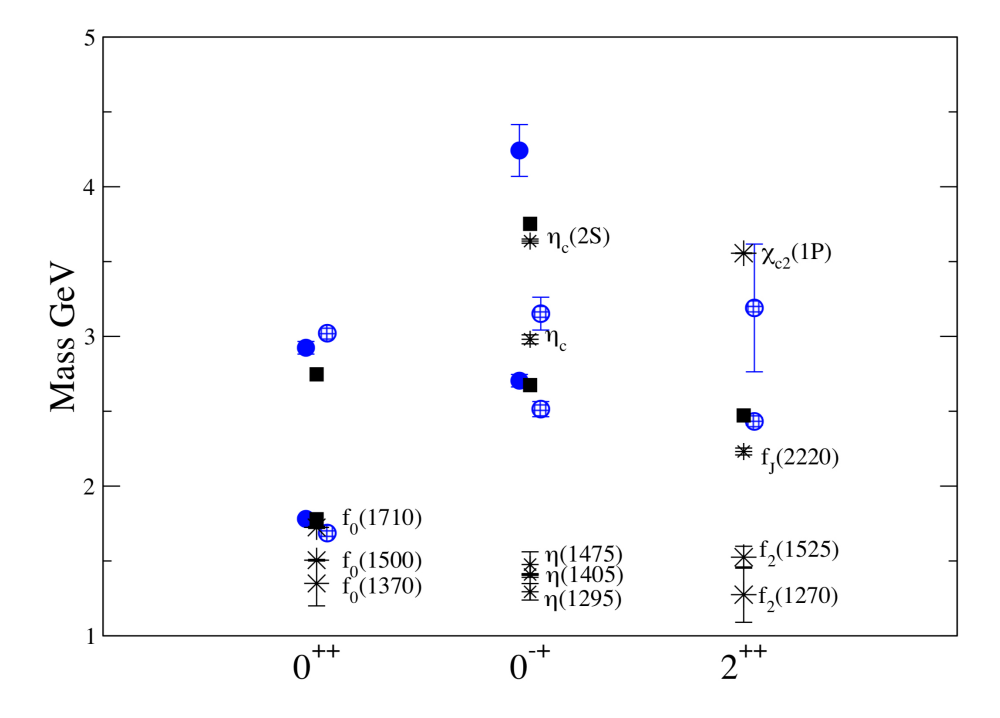


**Figure 15.15:** Lattice QCD predictions for glueball masses. The open and closed circles are the larger and smaller lattice spacing data of the full QCD calculation of glueball masses of Ref. [156], at pion masses of 280 and 360 MeV. Squares are the quenched data for glueball masses of Ref. [34]. The bursts labeled by particle names are experimental states with the appropriate quantum numbers.

channel, such as the rho coupled to two pions, have a large literature. An example of a calculation

of the rho meson decay width is [159]. (See also [160].) The mass and decay width of the  $f_0(500)$  have recently been computed in [161] and [162] and those of other mesons in [163]. Ref. [164] studies the decay width of the  $\Delta(1238)$ . A recent review [165] summarizes the lattice (and non-lattice) situation as of 2023.

Studies which observe a large basis of states across many volumes can probe excited state spectroscopy as resonances. These calculations are just beginning and the ones we know about are still performed at unphysically heavy quark masses. Examples include the decays of an exotic  $J^{PC} = 1^{-+}$  resonance [166] and the spectroscopy of  $J^{--}$  resonances [167]. The results of Refs. [144, 145] in Fig. 15.10 come from similar analyses. We expect to see considerable progress in this area over the next few years.

Some excited states are better thought of as bound states of hadrons. One example is the Lambda(1405), which is the subject of its own mini-review. Calculations with unitarized chiral perturbation theory (see, for example, Ref. [168] reveal a two-pole structure for the state. This structure has been confirmed starting directly from QCD by lattice simulations [169, 170].

We conclude this section with some remarks about unusual states containing heavy quarks. Lattice calculations relevant to the extra states observed in the charmonium and bottomonium spectrum (Sec. 15.4) are difficult, because the states sit high in the spectrum of most channels, because of the number of nearby multiparticle states, and because it is necessary to have the technology to study heavy and light quarks together.

Some lattice calculations are used as input for phenomenological studies of hybrids. The theoretical motivation is that one can imagine states made of a heavy  $Q\bar{Q}$  pair along with excitations of light degrees of freedom, viewed as an excited states of the string connecting them. The analogy is to an excited state of a diatomic molecule. The heavy quark potential, the potential from orbitally excited gluon configurations, and the "string breaking" potential (from the interaction between static sources and static-light mesons) are used as inputs in Born - Oppenheimer and coupled channel calculations for systems whose constituents include heavy quarks and antiquarks. Examples of such calculations include Refs. [171–173].

The system with the largest lattice literature is a bound state of two heavy quarks and two light antiquarks, for example  $bb\bar{u}d$ . The story begins with the spectroscopy of doubly and triply charmed baryons in Fig. 15.12; the lattice calculations in that figure were performed in 2010 - 2017. In 2017 two groups of authors [174,175] realized that one could extrapolate from the masses of  $Q\bar{q}$ , Qqq, and QQq states (Q for a heavy quark,  $\bar{q}$  for a light antiquark) to predict the mass of a  $QQ\bar{q}\bar{q}$  tetraquark. The  $QQ\bar{q}\bar{q}$  state would be stable if the mass of the Q were heavy enough. (This basically arises because the QQ diquark is in an attractive color-triplet state and the effective binding energy scales as  $\alpha_s^2 m_Q$ .) The  $J^P = 1^+$   $bb\bar{u}d$  state was expected to be stable. Simultaneously, a lattice calculation [176] of the mass of a  $bb\bar{u}d$  state showed that it was below threshold to fall apart into a pair of B mesons. The  $I(J^P) = 0(1^+)$  state is predicted to be stable by about 128(26) MeV [177] or 189(10) MeV [176]. (These authors put the  $bb\bar{s}d$  state at 98 MeV below threshold.) These numbers are in reasonable agreement with phenomenological estimates from Refs. [174,175].

These states are easier for the lattice theorist to study than other exotics because they are the lightest single particle states in their channels. They are difficult because they are just barely bound, and the usual approximation for a lattice calculation of unphysically heavy light quarks tends to raise their mass. The calculations have to include multiple trial states: the tetraquark itself plus pairs of mesons.

The situation with regard to the recently discovered  $T_{cc}(3875)^+$  [178] is still unsettled. Both lattice calculations and HQET estimates put a  $cc\bar{u}d$  state right at threshold, which is a difficult place to explore on the lattice (or by any other method, for that matter). The  $T_{cc}(3875)^+$  is seen in  $D^0D^0\pi^+$  and researchers studying three body decays on the lattice (an open problem, at present)

mark it as an obvious research target. One representative group describes their approach to the problem in Ref. [179].

#### 15.8.3 Electromagnetic effects

As a final part of spectroscopy we mention electromagnetic mass splittings (such as the neutron - proton mass difference). They are interesting but difficult. These calculations are important for determining the values of the quark masses (for a discussion see Sec. 60 in this Review). Knowing that the neutron is heavier than the proton tells us that these splittings have a complicated origin. One part of the shift is because the up and down quarks have slightly different masses. The second is that the quarks have (different) charges. Phenomenologists (compare Ref. [180]) combine Coulomb forces and spin-dependent electromagnetic hyperfine interactions to model their charge effects. In order to compute hadronic mass differences on the lattice, electromagnetic interactions must be included in the simulations. This creates a host of technical issues. An important one is that electromagnetic interactions are long range, but lattice simulations are done in finite volumes. The theoretical situation is summarized in the recent Flavour Lattice Averaging Group (FLAG) review [181]. A 2014 calculation, Ref. [182], presented the first results for electromagnetic mass splittings in the baryon octet, with good agreement with observation. Refs. [183–185] have performed calculations for meson splittings.

There is a small lattice literature associated with magnetic moments of baryons. The calculations are done by including a static magnetic field in the simulation and computing the energy difference between baryons in different spin states. We are aware of no calculations at physical quark masses. A recent calculation [186] used 800 and 450 MeV pions. When expressed in units of the nucleon magneton at the simulation point  $(e/(2M_N(m_\pi)))$  the moments are in reasonable agreement with experiment and with quark model expectations.

#### References

- [1] M.-L. Du et al., Phys. Rev. D 98, 094018 (2018), [arXiv:1712.07957].
- [2] G. 't Hooft, Nucl. Phys. B **72**, 461 (1974).
- [3] G. 't Hooft, Nucl. Phys. B **75**, 461 (1974).
- [4] E. Witten, Nucl. Phys. B **160**, 57 (1979).
- [5] F. Gross et al., Eur. Phys. J. C 83, 1125 (2023), [arXiv:2212.11107].
- [6] C. Amsler in the Quark Structure of Hadrons, Lecture Notes in Physics 949 (2018), ed. Springer.
- [7] H.-Y. Cheng, Physics Letters B **707**, 116 (2012), [arXiv:1110.2249].
- [8] J.-C. Feng et al., Phys. Rev. D 104, 054027 (2021), [arXiv:2104.01339].
- [9] H.-W. Ke and X.-Q. Li, Phys. Rev. D **99**, 036014 (2019), [arXiv:1810.07912].
- [10] M.-C. Du and Q. Zhao, Phys. Rev. D **100**, 036005 (2019), [arXiv:1905.04207].
- [11] A. A. Godizov, Eur. Phys. J. C **76**, 361 (2016), [arXiv:1604.01689].
- [12] S. Donnachie *et al.*, *Pomeron Physics and QCD*, Cambridge Monographs on Particle Physics, Nuclear Physics and Cosmology, Cambridge University Press, p. 85 (2002).
- [13] M.-L. Du et al., Phys. Rev. Lett. 126, 192001 (2021), [arXiv:2012.04599].
- [14] J. Schwinger, Phys. Rev. **135**, B816 (1964).
- [15] H. J. Lipkin and B.-s. Zou, Phys. Rev. D 53, 6693 (1996).
- [16] A. Bramon, R. Escribano and M. D. Scadron, Phys. Lett. B403, 339 (1997), [hep-ph/9703313].
- [17] A. Aloisio et al. (KLOE), Phys. Lett. **B541**, 45 (2002), [hep-ex/0206010].

- [18] F. Ambrosino et al., JHEP 07, 105 (2009), [arXiv:0906.3819].
- [19] C. Amsler et al. (Crystal Barrel), Phys. Lett. **B294**, 451 (1992).
- [20] C. Amsler, Rev. Mod. Phys. **70**, 1293 (1998), [hep-ex/9708025].
- [21] N. H. Christ et al., Phys. Rev. Lett. 105, 241601 (2010), [arXiv:1002.2999].
- [22] T. Feldmann, Int. J. Mod. Phys. **A915**, 159 (2000).
- [23] C. Amsler and F. E. Close, Phys. Rev. **D53**, 295 (1996), [hep-ph/9507326].
- [24] R. L. Jaffe, Phys. Rev. **D15**, 267 (1977).
- [25] R. L. Jaffe, Phys. Rev. **D15**, 281 (1977).
- [26] S.L. Olsen, Front. Phys. **10**, 121 (2015), [arXiv:1411.7738].
- [27] S. L. Olsen, T. Skwarnicki and D. Zieminska, Rev. Mod. Phys. 90, 015003 (2018), [arXiv:1708.04012].
- [28] N. Brambilla et al., Physics Reports 873, 1 (2020), [arXiv:1907.07583].
- [29] N. Hüsken, E. Norella and I. Polyakov, Modern Physics Letters A 40, 17n18, 2530002 (2025), [arXiv:2410.06923].
- [30] S. K. Choi et al., Physical Review Letters 91, 262001 (2003), [hep-ex/0309032].
- [31] N. A. Törnqvist, Physical Review Letters 67, 556 (1991).
- [32] R. Aaij et al., Nature Physics 18, 751 (2022), [arXiv:2109.01038].
- [33] R. Aaij et al., Science Bulletin 65, 1983 (2020), [arXiv:2006.16957].
- [34] C. J. Morningstar and M. J. Peardon, Phys. Rev. **D60**, 034509 (1999), [hep-lat/9901004].
- [35] Y. Chen et al., Phys. Rev. **D73**, 014516 (2006), [hep-lat/0510074].
- [36] W.-J. Lee and D. Weingarten, Phys. Rev. **D61**, 014015 (2000), [hep-lat/9910008].
- [37] G. S. Bali et al. (UKQCD), Phys. Lett. **B309**, 378 (1993), [hep-lat/9304012].
- [38] C. Michael, AIP Conf. Proc. 432, 657 (1998), [hep-ph/9710502].
- [39] A. Athenodorou and M. Teper, Journal of High Energy Physics **2020**, 11, 172 (2020), [arXiV:2007.06422].
- [40] J. Leutgeb and A. Rebhan, Phys. Rev. D 101, 014006 (2020), [arXiv:1909.12352].
- [41] F. Brünner, J. Leutgeb and A. Rebhan, Physics Letters B 788, 431 (2019), [arXiv:1807.10164].
- [42] M. Huber, C. S. Fischer and H. Sanchis-Alepuz, The European Physical Journal C 80, 11, 1077 (2020), [arXiv:2004.00415].
- [43] F. E. Close and A. Kirk, Eur. Phys. J. **C21**, 531 (2001), [hep-ph/0103173].
- [44] A. V. Sarantsev et al., Physics Letters B 816, 136227 (2021), [arXiv:2103.09680].
- [45] W. Ochs, J. Phys. **G40**, 043001 (2013), [arXiv:1301.5183].
- [46] F. Brünner and A. Rebhan, Phys. Rev. Lett. 115, 131601 (2015), [arXiv:1504.05815].
- [47] C. Amsler and N. A. Tornqvist, Phys. Rept. 389, 61 (2004).
- [48] N. Isgur and J. E. Paton, Phys. Rev. **D31**, 2910 (1985).
- [49] M. S. Chanowitz and S. R. Sharpe, Nucl. Phys. B222, 211 (1983), [Erratum: Nucl. Phys.B228,588(1983)].
- [50] T. Barnes et al., Nucl. Phys. **B224**, 241 (1983).
- [51] P. Lacock et al. (UKQCD), Phys. Lett. **B401**, 308 (1997), [hep-lat/9611011].
- [52] J. J. Dudek, Phys. Rev. D 84, 074023 (2011), [arXiv:1106.5515].

- [53] J. J. Dudek et al. (Hadron Spectrum), Phys. Rev. **D88**, 094505 (2013), [arXiv:1309.2608].
- [54] B. Kopf et al., The European Physical Journal C 81, 1056 (2021), [arXiv:2008.11566].
- [55] M. Ablikim et al. (BESIII), Phys. Rev. Lett. 129, 192002 (2022), [Erratum: Phys.Rev.Lett. 130, 159901 (2023)], [arXiv:2202.00621].
- [56] E. S. Swanson, Physical Review D 107, 074028 (2023), [arXiv:2302.01372].
- [57] R. Aaij et al. (LHCb), Phys. Rev. Lett. 115, 072001 (2015), [arXiv:1507.03414].
- [58] R. Aaij et al. (LHCb), Phys. Rev. Lett. 122, 222001 (2019), [arXiv:1904.03947].
- [59] A. V. Popov et al., Physics of Atomic Nuclei 83, 9, 1383 (2020).
- [60] J.-J. Wu et al., Phys. Rev. Lett. 105, 232001 (2010), [arXiv:1007.0573].
- [61] J.-J. Wu, T.-S. H. Lee and B. S. Zou, Phys. Rev. C 85, 044002 (2012), [arXiv:1202.1036].
- [62] Y.-R. Liu et al., Prog. Part. Nucl. Phys. 107, 237 (2019), [arXiv:1903.11976].
- [63] F.E. Close, in Quarks and Nuclear Forces (Springer-Verlag, 1982), p. 56.
- [64] R.H. Dalitz and L.J. Reinders, in "Hadron Structure as Known from Electromagnetic and Strong Interactions," *Proceedings of the Hadron '77 Conference* (Veda, 1979), p. 11.
- [65] E. Klempt and J.-M. Richard, Rev. Mod. Phys. 82, 1095 (2010), [arXiv:0901.2055].
- [66] T. Melde, W. Plessas and B. Sengl, Phys. Rev. **D77**, 114002 (2008), [arXiv:0806.1454].
- [67] N. Isgur and G. Karl, Phys. Rev. **D18**, 4187 (1978).
- [68] N. Isgur and G. Karl, Phys. Rev. **D19**, 2653 (1979), [Erratum: Phys. Rev. D23,817(1981)].
- [69] S. Capstick and W. Roberts, Prog. Part. Nucl. Phys. 45, S241 (2000), [arXiv:nucl-th/0008028].
- [70] S. Capstick and W. Roberts, Phys. Rev. **D58**, 074011 (1998), [arXiv:nucl-th/9804070].
- [71] S. Capstick, Phys. Rev. **D46**, 2864 (1992).
- [72] R. A. Arndt et al., Phys. Rev. C74, 045205 (2006), [arXiv:nucl-th/0605082].
- [73] B. Krusche and S. Schadmand, Prog. Part. Nucl. Phys. 51, 399 (2003), [arXiv:nucl-ex/0306023].
- [74] A. V. Anisovich et al., Eur. Phys. J. A52, 284 (2016), [arXiv:1604.05704].
- [75] E. Gutz et al. (CBELSA/TAPS), Eur. Phys. J. A50, 74 (2014), [arXiv:1402.4125].
- [76] V. Sokhoyan et al. (CBELSA/TAPS), Eur. Phys. J. A51, 95 (2015), [Erratum: Eur. Phys. J.A51,no.12,187(2015)], [arXiv:1507.02488].
- [77] E. Klempt et al., Eur. Phys. J. **A56**, 261 (2020), [arXiv:2007.04232].
- [78] J. Yelton et al. (Belle), Phys. Rev. Lett. 121, 5, 052003 (2018), [arXiv:1805.09384].
- [79] M. Ablikim et al. (BESIII), Phys. Rev. Lett. **134**, 13, 131903 (2025), [arXiv:2411.11648].
- [80] M. Sumihama et al. (Belle Collaboration), Phys. Rev. Lett. 122, 072501 (2019), [arXiv:1810.06181].
- [81] R. Aaij et al. (LHCb), Sci. Bull. 66, 1278 (2021), [arXiv:2012.10380].
- [82] V. Crede and J. Yelton, Rept. Prog. Phys. 87, 10, 106301 (2024), [arXiv:2502.08815].
- [83] G. Barucca et al., Eur. Phys. J. **A57**, 149 (2021).
- [84] G. Barucca et al., Eur. Phys. J. **A57**, 154 (2021).
- [85] S. Capstick and W. Roberts, Prog. in Part. Nucl. Phys. 45, 241 (2000), [arXiv:nucl-th/0008028].

- [86] V. Crede and W. Roberts, Rept. on Prog. in Phys. **76**, 076301 (2013), [arXiv:1302.7299].
- [87] M. Ferraris et al., Phys. Lett. **B364**, 231 (1995).
- [88] M. M. Giannini and E. Santopinto, Chin. J. Phys. 53, 020301 (2015), [arXiv:1501.03722].
- [89] M. Anselmino et al., Rev. Mod. Phys. 65, 1199 (1993).
- [90] R. Bijker, F. Iachello and A. Leviatan, Annals Phys. 236, 69 (1994), [arXiv:nucl-th/9402012].
- [91] S. Capstick and P. R. Page, Phys. Rev. C66, 065204 (2002), [arXiv:nucl-th/0207027].
- [92] R. L. Jaffe, D. Pirjol and A. Scardicchio, Phys. Rept. 435, 157 (2006), [hep-ph/0602010].
- [93] G. Eichmann et al., Prog. Part. Nucl. Phys. 91, 1 (2016), [arXiv:1606.09602].
- [94] G. Eichmann and C. S. Fischer, Few Body Syst. **60**, 2 (2019).
- [95] A. Bashir et al., Commun. Theor. Phys. 58, 79 (2012), [arXiv:1201.3366].
- [96] C. D. Roberts, IRMA Lect. Math. Theor. Phys. 21, 355 (2015).
- [97] R. Slansky, Phys. Rept. **79**, 1 (1981).
- [98] M. Karliner and J. L. Rosner, Phys. Rev. **D90**, 094007 (2014), [arXiv:1408.5877].
- [99] M. Ablikim et al. (BESIII), Phys. Rev. D 103, 9, L091101 (2021), [arXiv:2011.00396].
- [100] R. Aaij et al. (LHCb), Phys. Rev. Lett. 118, 182001 (2017), [arXiv:1703.04639].
- [101] R. Aaij et al. (LHCb), Phys. Rev. Lett. 131, 13, 131902 (2023), [arXiv:2302.04733].
- [102] Y. Yelton et al., Phys. Rev. **D97**, 051102(R) (2018).
- [103] R. Aaij et al., Phys. Rev. Lett **124**, 082002 (2020).
- [104] R. Aaij et al. (LHCb), Phys. Rev. Lett. 119, 112001 (2017), [arXiv:1707.01621].
- [105] R. Aaij et al. (LHCb), Phys. Rev. Lett. **121**, 16, 162002 (2018), [arXiv:1807.01919].
- [106] R. Aaij et al. (LHCb), JHEP **05**, 038 (2022), [arXiv:2202.05648].
- [107] M. Mattson et al. (SELEX), Phys. Rev. Lett. 89, 112001 (2002), [hep-ex/0208014].
- [108] A. Ocherashvili et al. (SELEX), Phys. Lett. **B628**, 18 (2005), [hep-ex/0406033].
- [109] R. Aaij et al. (LHCb), Sci. China Phys. Mech. Astron. 63, 221062 (2020), [arXiv:1909.12273].
- [110] S. Brodsky, S. Groote and S. Koshkarev, Eur. Phys. J. C78, 483 (2018).
- [111] R. Aaij et al. (LHCb), JHEP **05**, 030 (2017), [arXiv:1701.07873].
- [112] R. Aaij et al. (LHCb), Phys. Rev. Lett. 131, 17, 171901 (2023), [arXiv:2307.13399].
- [113] A. M. Sirunyan et al. (CMS), Phys. Rev. Lett. 126, 25, 252003 (2021), [arXiv:2102.04524].
- [114] L. Schachinger et al., Phys. Rev. Lett. 41, 1348 (1978).
- [115] G. Lopez Castro and A. Mariano, Physics Letters B **517**, 3, 339 (2001), [arXiv:nucl-th/0006031].
- [116] A. Morelos Pineda et al. (E761), Phys. Rev. Lett. **71**, 3417 (1993).
- [117] D. W. Hertzog et al., Phys. Rev. D 37, 1142 (1988).
- [118] N. B. Wallace et al., Phys. Rev. Lett. **74**, 3732 (1995).
- [119] A. Bosshard et al., Phys. Rev. D 44, 1962 (1991).
- [120] M. Kotulla et al., Phys. Rev. Lett 27, 272001 (2002).
- [121] S. Schumann et al., The European Physical Journal A 43, 269 (2010).
- [122] A. De Rujula, H. Georgi and S. L. Glashow, Phys. Rev. **D12**, 147 (1975).
- [123] W. H. Blask et al., Z. Phys. **A337**, 327 (1990).

- [124] U. Loring et al., Eur. Phys. J. A10, 309 (2001), [hep-ph/0103287].
- [125] L. Ya. Glozman and D. O. Riska, Phys. Rept. 268, 263 (1996), [hep-ph/9505422].
- [126] T. DeGrand and E. T. Neil, Phys. Rev. D **101**, 034504 (2020), [arXiv:1910.08561].
- [127] C. Aubin et al., Phys. Rev. **D70**, 094505 (2004), [hep-lat/0402030].
- [128] A. Bazavov et al. (MILC), Rev. Mod. Phys. 82, 1349 (2010), [arXiv:0903.3598].
- [129] S. Aoki et al. (PACS-CS), Phys. Rev. **D79**, 034503 (2009), [arXiv:0807.1661].
- [130] S. Durr et al., Science **322**, 1224 (2008), [arXiv:0906.3599].
- [131] W. Bietenholz et al., Phys. Rev. **D84**, 054509 (2011), [arXiv:1102.5300].
- [132] C. Alexandrou et al., Phys. Rev. **D90**, 074501 (2014), [arXiv:1406.4310].
- [133] J. J. Dudek et al., Phys. Rev. **D83**, 111502 (2011), [arXiv:1102.4299].
- [134] E. B. Gregory et al. (UKQCD), Phys. Rev. **D86**, 014504 (2012), [arXiv:1112.4384].
- [135] C. Michael, K. Ottnad and C. Urbach (ETM), Phys. Rev. Lett. 111, 181602 (2013), [arXiv:1310.1207].
- [136] C. Bernard *et al.* (Fermilab Lattice, MILC), Phys. Rev. **D83**, 034503 (2011), [arXiv:1003.1937].
- [137] E. B. Gregory et al., Phys. Rev. **D83**, 014506 (2011), [arXiv:1010.3848].
- [138] R. J. Dowdall et al., Phys. Rev. **D86**, 094510 (2012), [arXiv:1207.5149].
- [139] D. Mohler and R. M. Woloshyn, Phys. Rev. **D84**, 054505 (2011), [arXiv:1103.5506].
- [140] A. S. Kronfeld, Ann. Rev. Nucl. Part. Sci. 62, 265 (2012), [arXiv:1203.1204].
- [141] K. Ottnad, C. Urbach and F. Zimmermann (OTM), Nucl. Phys. **B896**, 470 (2015), [arXiv:1501.02645].
- [142] G. S. Bali et al. (RQCD), JHEP 08, 137 (2021), [arXiv:2106.05398].
- [143] C. DeTar *et al.* (Fermilab Lattice, MILC), Phys. Rev. D **99**, 034509 (2019), [arXiv:1810.09983].
- [144] S. Piemonte et al., Phys. Rev. D 100, 074505 (2019), [arXiv:1905.03506].
- [145] S. Prelovsek et al., JHEP **06**, 035 (2021), [arXiv:2011.02542].
- [146] M. Padmanath, C. B. Lang and S. Prelovsek, Phys. Rev. D **92**, 034501 (2015), [arXiv:1503.03257].
- [147] L. Liu et al., Phys. Rev. **D81**, 094505 (2010), [arXiv:0909.3294].
- [148] R. A. Briceno, H.-W. Lin and D. R. Bolton, Phys. Rev. **D86**, 094504 (2012), [arXiv:1207.3536].
- [149] Y. Namekawa et al. (PACS-CS), Phys. Rev. **D87**, 094512 (2013), [arXiv:1301.4743].
- [150] M. Padmanath et al., Phys. Rev. **D90**, 074504 (2014), [arXiv:1307.7022].
- [151] Z. S. Brown *et al.*, Phys. Rev. **D90**, 094507 (2014), [arXiv:1409.0497].
- [152] P. Pérez-Rubio, S. Collins and G. S. Bali, Phys. Rev. **D92**, 034504 (2015), [arXiv:1503.08440].
- [153] C. Alexandrou and C. Kallidonis, Phys. Rev. **D96**, 034511 (2017), [arXiv:1704.02647].
- [154] S. Meinel, private comunication.
- [155] R. G. Edwards et al., Phys. Rev. **D84**, 074508 (2011), [arXiv:1104.5152].
- [156] C. M. Richards et al. (UKQCD), Phys. Rev. **D82**, 034501 (2010), [arXiv:1005.2473].
- [157] E. Gregory et al., JHEP 10, 170 (2012), [arXiv:1208.1858].

- [158] C. Morningstar, PoS LATTICE2024, 004 (2024), [arXiv:2502.02547].
- [159] J. Bulava et al., Nucl. Phys. **B910**, 842 (2016), [arXiv:1604.05593].
- [160] A. Rodas, J. J. Dudek and R. G. Edwards (Hadron Spectrum), Phys. Rev. D 108, 3, 034513 (2023), [arXiv:2303.10701].
- [161] R. A. Briceno et al., Phys. Rev. Lett. 118, 022002 (2017), [arXiv:1607.05900].
- [162] D. Guo et al., Phys. Rev. D 98, 014507 (2018), [arXiv:1803.02897].
- [163] R. A. Briceno et al., Phys. Rev. D 97, 5, 054513 (2018), [arXiv:1708.06667].
- [164] J. Bulava et al., Nucl. Phys. B 987, 116105 (2023), [arXiv:2208.03867].
- [165] M. Mai, U.-G. Meißner and C. Urbach, Phys. Rept. **1001**, 1 (2023), [arXiv:2206.01477].
- [166] A. J. Woss et al. (Hadron Spectrum), Phys. Rev. D 103, 054502 (2021), [arXiv:2009.10034].
- [167] C. T. Johnson and J. J. Dudek (Hadron Spectrum), Phys. Rev. D 103, 074502 (2021), [arXiv:2012.00518].
- [168] J. A. Oller and U. G. Meissner, Phys. Lett. B **500**, 263 (2001), [hep-ph/0011146].
- [169] J. Bulava *et al.* (Baryon Scattering (BaSc)), Phys. Rev. Lett. **132**, 5, 051901 (2024), [arXiv:2307.10413].
- [170] J. Bulava et al. (Baryon Scattering (BaSc)), Phys. Rev. D 109, 1, 014511 (2024), [arXiv:2307.13471].
- [171] R. Bruschini and P. González, Phys. Rev. D **102**, 074002 (2020), [arXiv:2007.07693].
- [172] R. Bruschini and P. González, Phys. Rev. D 103, 074009 (2021), [arXiv:2101.04636].
- [173] R. F. Lebed, R. E. Mitchell and E. S. Swanson, Prog. Part. Nucl. Phys. 93, 143 (2017), [arXiv:1610.04528].
- [174] E. J. Eichten and C. Quigg, Phys. Rev. Lett. 119, 202002 (2017), [arXiv:1707.09575].
- [175] M. Karliner and J. L. Rosner, Phys. Rev. Lett. 119, 202001 (2017), [arXiv:1707.07666].
- [176] A. Francis et al., Phys. Rev. Lett. 118, 142001 (2017), [arXiv:1607.05214].
- [177] L. Leskovec et al., Phys. Rev. D 100, 014503 (2019), [arXiv:1904.04197].
- [178] R. Aaij et al. (LHCb), Nature Phys. 18, 751 (2022), [arXiv:2109.01038].
- [179] S. M. Dawid, F. Romero-López and S. R. Sharpe, JHEP **01**, 060 (2025), [arXiv:2409.17059].
- [180] M. Karliner and J. L. Rosner **100**, 073006 (2019), [arXiv:1906.07799].
- [181] Y. Aoki et al. (Flavour Lattice Averaging Group (FLAG)), Eur. Phys. J. C 82, 869 (2022), [arXiv:2111.09849].
- [182] S. Borsanyi et al., Science **347**, 1452 (2015), [arXiv:1406.4088].
- [183] G. M. de Divitiis et al. (RM123), Phys. Rev. D 87, 114505 (2013), [arXiv:1303.4896].
- [184] D. Giusti et al., Phys. Rev. **D95**, 114504 (2017), [arXiv:1704.06561].
- [185] S. Basak *et al.* (MILC), Phys. Rev. D **99**, 034503 (2019), [arXiv:1807.05556].
- [186] A. Parreno et al., Phys. Rev. D 95, 114513 (2017), [arXiv:1609.03985].